

Dear Editor

We are grateful to you and two reviewers for the helpful comments on the previous version of our manuscript. We have addressed all the comments made by two reviewers, as follows. Generally, we revised the manuscript according to reviewer's comments. This is because the comments of all reviewers are very useful for improving our manuscript and strengthening the interpretation of our model results. Native speaker has performed proofreading of our manuscript and corrected errors and inappropriate expression in English sentences. We hope that the revised version of our paper is now suitable for publication in *Climate of the Past*.

Response to Fortunat Joos (Referee)

(Our response **highlighted gray**.)

**General comment:**

Yamamoto and colleagues present an interesting analysis of glacial change in atmospheric CO<sub>2</sub> and marine oxygen. The authors investigate, using a range of factorial analyses, the impacts of glaciogenic iron input and an increased nutrient inventory in the glacial ocean. They apply an offline biogeochemical model for Last Glacial Maximum (LGM) and preindustrial (PI) conditions. They simulate an upper limit for the CO<sub>2</sub> decrease due to iron fertilization of 20 ppm and a similar decrease due to an increase in whole ocean nutrient inventory. They present a novel model-proxy comparison for PI-LGM changes in O<sub>2</sub>. The results suggest a role of iron fertilization and changes in nutrient inventory for low glacial CO<sub>2</sub> and for the reconstructed oxygen changes. The manuscript is concise and well written. Figures and tables are illustrative and support the conclusions.

I recommend publication of the manuscript after minor revision.

**Response: We appreciate the positive recommendation and helpful comments from Professor Fortunat Joos. We reply to each specific comment below.**

Comment #1

I find it interesting that the upper limit for iron fertilization is 20 ppm (p10, l215). I would appreciate if this finding is lifted to the abstract.

**Response: Thank you very much for this positive comment. We also think that this result is interesting. However, as mentioned by another referee (Professor Andreas Schmittner), there remains a possibility that**

**this upper limit for iron fertilization is not a robust result because present iron models have a large uncertainty. Thus, we do not mention the upper limit of iron fertilization in the abstract. To obtain a deeper understanding of the impact of iron fertilization on glacial CO<sub>2</sub> decrease, the variability of upper limit among iron models should be investigated in the future study.**

Comment #2

Figure 8 shows results from WOA2009 and simulated anomalies. Results for the model for the modern ocean should be displayed as well. This would permit the reader to assess the quality of the simulated O<sub>2</sub> field.

**Response: According to the reviewer's comment, we added the simulated O<sub>2</sub> distribution for the modern ocean to Figure 8. The following figure and caption are the revised version of Figure 8.**

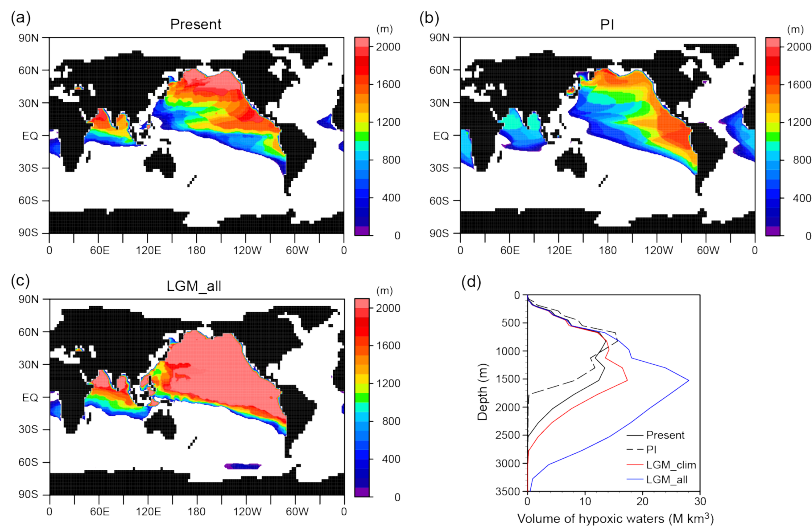


**Figure 8. Hypoxic waters expansion. Horizontal distribution of thickness of the hypoxic waters ( $[O_2] < 80 \text{ mmol m}^{-3}$ ) for the (a) present, (b) PI, and (c) LGM\_all. (d) Vertical distribution of hypoxic waters for the present (black solid), PI (black dashed), LGM\_clim (red), and LGM\_all (blue). Because current coarse**

**resolution models have difficulties reproducing low oxygen concentration for the present day (Bopp et al., 2013), observed values from WOA2009 (Garcia et al., 2010a) were used for the present. For the LGM simulations, we combined the observed values with the modelled changes.**

Comment #3

There are some language problems, e.g. missing articles, and the manuscript would benefit from proof-reading by a native speaker.

**Response: A native speaker have performed proof-reading of our manuscript.**

Comment #4

There is no discussion on the role of the burial-nutrient feedback and how burial-nutrient feedback may affect the results of this study. On page 10, l221, it is mentioned that CaCO<sub>3</sub> compensation is not included. However, this study does also not consider how changes in iron fertilization affect the balance between weathering and burial of organic matter. This also applies to some extent to the experiment with the increase in whole ocean nutrient inventory.

Several studies point to the potentially important role of the ocean/sediment/lithosphere fluxes of organic matter and how the associated burial-nutrient feedback modifies the magnitude and time scales of the response in CO<sub>2</sub> and other tracers to changes in the marine biological cycles (Wallmann et al., 2016; Roth et al., 2014; Jeltsch-Thömmes et al., 2018). (Tschumi et al., 2011), for example, quantify the implication of ocean-sediment-lithosphere coupling for an experiment where the ocean P inventory is increased. (Menviel et al., 2012) present results from factorial experiments with altered iron fertilization/dust input and altered P inventory plus variation in other drivers from transient glacial-interglacial simulations. I suggest that this caveat is addressed on page 10 and perhaps also in the discussion section.

**Response: Thank you for your useful suggestion. We added the following discussion about the role of the burial-nutrient feedback to page11, L246-257 in the revised manuscript.**

**“Note that changes in the sedimentation process (i.e. carbonate compensation and burial-nutrient feedback) are not considered in our simulation. The simulated increase in the bottom water DIC (Fig. 4) would enhance**

calcium carbonate dissolution in the sediments and thereby increase ocean alkalinity, leading to a further CO<sub>2</sub> decrease (Bouttes et al., 2011; Brovkin et al., 2012; Kobayashi et al., 2018). The long-term balance between the burial of organic material and nutrient input through weathering is also potentially important for the response in atmospheric CO<sub>2</sub> and related tracers to changes in ocean biological cycles (Roth et al., 2014; Wallmann et al., 2016). For example, Tschumi et al. (2011) show that the nutrient-burial feedback significantly amplifies the effect of an increase in the PO<sub>4</sub> inventory on the glacial CO<sub>2</sub> decrease. Menviel et al. (2012) quantified the implication of ocean-sediment-lithosphere coupling for factorial experiments with an altered iron fertilization and altered PO<sub>4</sub> inventory from transient glacial-interglacial simulations. Considering that EP increases due to iron fertilization and the nutrient increase is smaller in our simulations than that in previous studies (Tschumi et al., 2011; Menviel et al., 2012), the effect of burial-nutrient feedback on the glacial CO<sub>2</sub> reduction may be smaller than previously estimated.”

Minor and technical comments

#1

P1, line 11, p3, l46: “.. due to sea surface cooling” What matters is in my opinion the cooling of the whole ocean, including the ocean interior. Please modify the wording

**Response: “due to sea surface cooling” was changed to “due to seawater cooling” in page1 L10-11 in the revised manuscript.**

#2

P1, l16-18: This sentence is not so clear. The circulation changes itself likely induce a change in the efficiency of the biological pump (Volk and Hoffert, 1985) as may also be seen when looking at preformed/remineralized nutrients or AOU. I think it should rather read “whereas the other half is driven by iron fertilization and an increase in whole ocean P inventory” or similar.

**Response: We agree fully with the referee on this point. We revised this sentence as follow (page1 L16-18). “Sensitivity experiments show that physical changes contribute to only one-half of all glacial deep deoxygenation whereas the other one-half is driven by iron fertilization and an increase in the whole ocean nutrient inventory.”**

#3

P5, 190: Is convection included in the offline model and how is this done?

**Response: Yes, effects of convection are included in offline model by enhancing the value of the vertical diffusivity where the convection takes place.**

#4

P9, 1192, You may also refer to (Menviel et al., 2012)

#5

P8, 1182: missing word: "shortwave radiation"

#6

P10, 1207: you may include here EMICs results (e.g. (Muglia et al., 2017; Parekh et al., 2008; Menviel et al., 2012;Heinze et al., 2016).

**Response: As for these three comments, we added the suggested reference and missing word to the revised manuscript (page10 207, page9 L195, page10 L226-228). We would like to thank the reviewer for the attention to detail.**

Response to Andreas Schmittner (Referee)

(Our response **highlighted gray.**)

**General comment:**

Yamamoto and co-workers present a nice modeling study of glacial ocean oxygen and carbon changes. The manuscript is well written (except for a few typos) and nicely illustrated. I think the main new finding is that glaciological iron sources from Patagonia are particularly important for lowering atmospheric CO<sub>2</sub>. Although similar suggestions have been made previously with simpler models (e.g. Brovkin et al., 2007) this study is the first to my knowledge that cleanly separates glaciological from other (desert) dust sources.

However, I have a few concerns that require revisions. Some of those concerns result from a study by Khatiwala et al. that is currently in review with Science Advances. We hope that it will be published soon so that the authors can access it and consider it in their revision.

**Response: We are grateful to Professor Andreas Schmittner for careful review and useful comments. The reviewer's comments are helpful for us to improve our manuscript. Referring to the comments, we carefully revised the manuscript. The specific replies are as follows.**

Comment #1

Khatiwala et al. use a data-constrained model of the LGM to decompose the carbon cycle. They show that using the AOU approximation to calculate respired carbon leads to large errors (even the wrong sign) in LGM – PI simulations. This conclusion is supported by previous studies who have demonstrated the errors in the AOU approximation (Russell et al., 2003; Ito et al., 2004; Duteil et al., 2013). For this reason, I would advise not to use it and remove the corresponding parts of the manuscript (e.g. in section 3.2).

**Response: We were not aware of these previous studies and agree that AOU contains errors. In the revised manuscript we did not remove section 3.2, but add the following annotation to page10 L218-221.**

**Notably, the AOU is different from true oxygen utilization due to the air-sea disequilibrium which is on the order of 20 mmol m<sup>-3</sup> in deep-water formation regions (Russell and Dickson, 2003; Duteil et al., 2013). Changes in surface ocean disequilibrium between the PI and LGM simulations might lead to large errors in the AOU changes.**

Comment #2

It is OK to refer to the iron fertilization effect as increasing the efficiency of the biological pump, but not that the LGM biological pump was enhanced. Khatiwala et al. show that the biological pump was not enhanced, but that air-sea disequilibrium was increased, which caused the glacial ocean carbon inventory to be larger.

**Response: According to the reviewer's comment, "enhanced biological pump" and "biological pump was enhanced" are removed in the revised manuscript.**

Comment #3

Air-sea disequilibrium was enhanced in the LGM not only for carbon but also for oxygen and radiocarbon. Khatiwala et al. show that in their best fitting model the ideal age of the whole ocean is younger, while the whole ocean c14-age is older due to the increased disequilibrium (or increased preformed c14-age). This is relevant for the discussion at the end of section 3 (lines 280-287) and the corresponding parts of the abstract (lines 22-24). Thus, ideal age and c14-age cannot be compared and there may not be a discrepancy here between modeled younger ideal age and older (observed) c14-age. I also think that one quantitative oxygen reconstruction from the Southern Ocean alone (Gottschalk et al. 2016) is not enough to indicate that the model is wrong. Reconstructions have errors and therefore I would not overemphasize this apparent discrepancy.

**Response: Thank you for sharing the manuscript. We did not add the discussion about the effect of air-sea disequilibrium on ideal age and c14-age because, at the moment, Khatiwala et al. has not been formally accepted.**

Comment #4

Another concern is the discussion of nutrient inventory changes. Somes et al. (2017) have considered this and shown that existing nitrogen isotope data provide no constraints on this effect. I'm also not aware of other observations supporting it (including evidence provided in this manuscript). For this reason, I think this effect remains unconstrained by observations and thus highly uncertain. I'd encourage the authors to reflect this uncertainty more in their discussion of this effect and to cite the above paper, which has also examined its effects on oxygen.

**Response: Thank you for your useful suggestion. As reviewer said, the discussion of nutrient inventory changes is necessary for our manuscript. We added the following discussion to the revised manuscript (page15 L335-339).**

**“The changes in nutrient inventory during the LGM have large uncertainties. Previous studies estimate that the oceanic PO<sub>4</sub> and NO<sub>3</sub> inventories could have been 15–40% (Tamburini and Föllmi, 2009; Wallmann et al., 2016) and 10-100% (Deutsch et al., 2004; Eugster et al., 2013; Somes et al., 2017) greater during glacial compared to interglacial periods, respectively. Moreover, Somes et al. (2017) shows that sedimentary δ<sup>15</sup>N**

**records provide no constrain on this effect. Future simulations should test the biogeochemical sensitivity to nutrient inventory changes.”**

Comment #5

The authors claim that their model fits reconstructions of export production by Kohfeld et al. (2005), which show not much change in the Pacific sector of the Southern Ocean. However, there are some newer data from that region by Studer et al. (2015) and Wang et al. (2017) that indicate increased nutrient utilization there as well. This suggests that the model underestimates iron fertilization in the Pacific sector of the Southern Ocean.

**Response: Thank you for information on new data. In addition to suggested references, we also found Kohfeld et al (2013) which include many reconstructions of export production in the Pacific sector of the Southern Ocean. We added these data to figure 3 and also revised page9 L195-203 as follow.**

**“In the model, the EP changes also have an east-west dipole pattern; slight EP increases are found in the South Pacific Ocean and significant EP increases occur in the South Atlantic and Indian oceans. We found that this pattern is attributed to iron fertilization by glaciogenic dust. Glaciogenic dust derived from Patagonian glaciers is transported to the South Atlantic and Indian oceans by the southern westerly wind; however, it is unable to reach the South Pacific (Fig. S3). Proxy data show no clear east-west dipole pattern, suggesting that the model underestimates iron fertilization in the Pacific sector of the Southern Ocean. However, proxy data in the South Pacific remain sparse and a quantitative comparison of EP changes between the South Atlantic and South Pacific is limited. Therefore, further proxy data in the South Pacific is required for a comprehensive understanding of the glacial EP changes and iron fertilization.”**

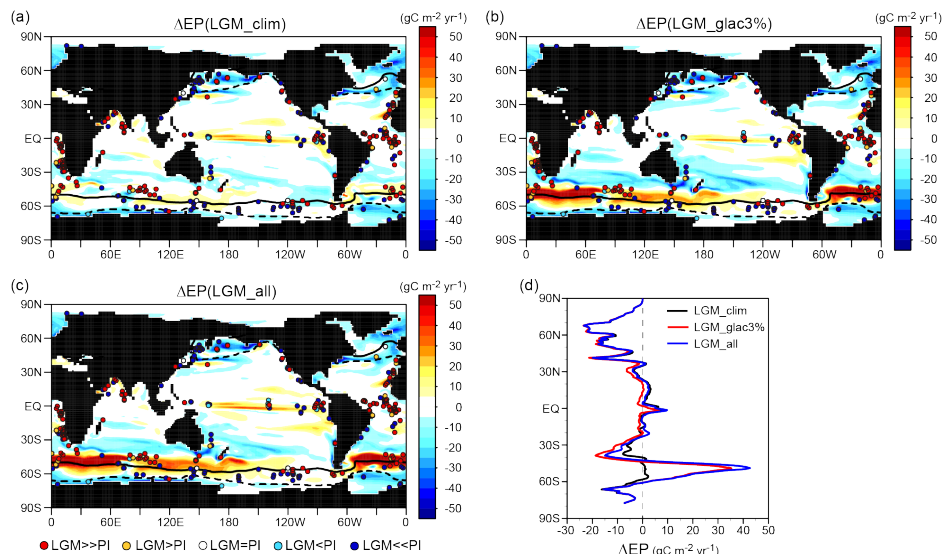


**Figure 3. Model-proxy comparison of EP change from the PI to LGM. The EP difference from the PI for (a) LGM\_clim, (b) LGM\_glac3%, and (c) LGM\_all. Circles show proxy data (Kohfeld et al., 2013). Solid (dotted) lines refer to the glacial sea ice fraction of 0.1 during August (February). (d) Zonal mean changes in the surface EP from the PI for LGM\_clim (black), LGM\_glac3% (red), and LGM\_all (blue).**

#### Comment #6

In any case, given the uncertainties in existing paleo data and iron models and solubility of iron, it is not fair to say that the upper limit of iron fertilization is 20 ppm as claimed here in lines 214-215. Khatiwala et al. suggest an iron effect of 35 ppm. Here I also disagree with Fortunat's suggestion to mention the CO<sub>2</sub> limit in the abstract. I don't think it is a robust result. However, the idea that the effect of iron fertilization is limited and that increasing fluxes will have a smaller effect at high fluxes than at low fluxes is robust and agrees with previous results (Muglia et al., 2018). The latter paper suggests this limitation is due to increased scavenging rather than reduced regions of iron limitation. Both seem plausible explanations.

**Response: Thank you for this discussion. We added the following discussion about the uncertainty of upper limit of iron fertilization to the revised manuscript (page11 L238-241).**

**“The simulated upper limit of CO<sub>2</sub> reduction resulting from iron fertilization is not a robust result because present iron models have large uncertainty. While Parekh et al. (2008) show an upper limit of 10 ppm, other simulations show CO<sub>2</sub> decrease by greater than 20 ppm (Oka et al., 2011; Muglia et al., 2017). To obtain a better understanding of the impact of iron fertilization on glacial CO<sub>2</sub> decrease, the variability of the upper limit among iron models should be investigated in a future study.”**

Minor and technical comments

#1

Line 16-17: I suggest to remove “(e.g. more sluggish ocean circulation)” because no such attribution was done in the paper. Khatiwala et al. suggest no CO<sub>2</sub> effect from ocean circulation changes.

**Response: According to the reviewer’s comment, we removed this part.**

#2

Line 17-18: I suggest to remove “enhanced efficiency of the biological pump” here for the above mentioned reasons.

**Response: In the revised text “by enhanced efficiency of the biological pump” was changed to “by iron fertilization and an increase in the whole ocean nutrient inventory”. (page1 L17-18)**

#3

Line 21: this sentence is awkward. I suggest to rephrase to “glacial deep water was a more severe environment for ... than the modern ocean.”

#4

Lines 24, 26: again, I’d suggest to rephrase to avoid using the term “biological pump” because it has not been quantified how much CO<sub>2</sub> change was due to biological pump changes. Perhaps better to use “iron fertilization and/or global nutrient increase”.

**Response: Thank you for pointing out. Following reviewer's comments, we corrected these two sentences. (page1 L21-22, page1 L24-25)**

#5

Line 31: the biological pump also includes the CaCO<sub>3</sub> pump

**Response: We changed “the biological pump” to “the soft-tissue biological pump”. (page3 L32)**

#6

Lines 50-51: consider including Schmittner and Somes (2015) and Somes et al. (2017)

**Response: Suggested references are added in the revised manuscript (page3 L52).**

#7

Lines 51-52: Khatiwala et al. have explored oxygen changes in more detail

**Response: We did not refer Khatiwala et al. because, at the moment, it has not been formally accepted.**

#8

Line 83: see above comments on “biological pump”

**Response: “enhanced efficiency of biological pump associated with” will be removed in the revised manuscript (page5 L84).**

#9

109-110: iron solubility is modified by transport in the atmosphere. This leads to increasing solubility at lower concentrations. This effect has been considered in Muglia et al. (2017; their Fig. 2). This suggests using a constant solubility is not correct. This should be discussed.

**Response: We agree that a constant solubility is not correct. We added the discussion about iron solubility to the revised manuscript (page6 L123-130), as follow.**

**“Present observation generally shows a lower Fe solubility at a higher Fe concentration in aerosols and a higher solubility at a lower concentration (Fig. S1). A wider range of aerosol Fe solubility (from 0.2% to 48%) has been derived from observations over the SO, but different types of Fe-containing minerals such as pyrogenic Fe oxides can be considered to achieve high Fe solubilities (Ito et al., 2019). Thus, an assumed constant iron solubility of 2% in all types of dust could lead to overestimation of a total DFe flux from different types of Fe-containing aerosols during the LGM (Muglia et al., 2017). However, a much higher Fe solubility (1–42% of Fe solubility) as derived from observations for the LGM aerosols in Antarctica has suggested that an assumed constant iron solubility of 1–2% for all types of dust could lead to a DFe flux underestimation during the LGM (Conway et al., 2015).”**

#10

116-119: This is about a factor of 10 increase in the 3% experiments. Compare with Muglia et al. (2018) who only have a factor of 4 increase in their best fitting model, which is constrained by  $\delta^{15}\text{N}$  and  $\delta^{13}\text{C}$  data.

**Response: We added following sentences to page7 L131-133 in the revised manuscript.**

**“This value is approximately 10 times larger than that of the PI simulation and is larger than a recent estimation, suggesting that a quadrupling of the global DFe flux is constrained by a model-proxy comparison of  $\delta^{15}\text{N}$  and  $\delta^{13}\text{C}$  (Muglia et al., 2018).”**

#11

129-130: Muglia et al. (2017) shows the sea level effect to be important.

**Response: “Muglia et al (2017) showed this effect causes  $\text{CO}_2$  increase of 15 ppm.” is added to page 7 L141-142.**

#12

General comment on section 2: how was the effect of sea level lowering on benthic denitrification treated? Some et al. (2017) show that this effect reduces N loss in the LGM ocean and leads to a larger N inventory.

**Response: Benthic denitrification is not considered in our model. We added this information to page8 L162-164, as follow.**

**“In our simulations, changes in benthic denitrification were not considered. *Somes et al. (2017)* show that a decrease in benthic denitrification because of a sea level drop reduces NO<sub>3</sub> loss and thus leads to a larger NO<sub>3</sub> inventory in the LGM ocean.”**

#13

165: delete: “because dust deposition flux of the Southern Ocean is underestimated in LGM\_dust”

#14

166: delete “in the” and “with iron limitation”

#15

167: delete “in the”

**Response: According to reviewer’s comments, we removed these three parts (page9 L179, page9 L180).**

#16

182-184: see above comment on new data from the S. Pacific

**Response: As mentioned above, we revised page9 L195-203 and compared our model with new data of the Southern Pacific.**

#17

199-201: see above comments on biological pump. I doubt that this conclusion is true because of the use of the AOU approximation here, which compromises the results.

**Response: As mentioned above, we added the annotation about errors of AOU approximation (page10 L218-221).**

#18

239: replace “is the one” with “may be one of the”. Or even better remove this whole part due to my above comments.

**Response: “is the one” was changed to “may be one of the” (page12 L271).**

#19

243: typo: “whehre”

**Response: Thank you for pointing out. We fixed typo in the revised manuscript.**

References:

Kohfeld, K. E., Graham, R. M., de Boer, A. M., Sime, L. C., Wolff, E. W., Le Quéré, C., and Bopp, L.: Southern Hemisphere westerly wind changes during the last glacial maximum: Paleo-data synthesis, *Quat. Sci. Rev.*, 68, 76–95, 2013.

Parekh, P., Joos, F., and Muller, S. A.: A modeling assessment of the interplay between aeolian iron fluxes and ironbinding ligands in controlling carbon dioxide fluctuations during Antarctic warm events, *Paleoceanography*, 23, Pa4202, doi:10.1029/2007pa001531, 2008.

# Glacial CO<sub>2</sub> decrease and deep-water deoxygenation by iron fertilization from glaciogenic dust

Akitomo Yamamoto<sup>1,2</sup>, Ayako Abe-Ouchi<sup>1,2</sup>, Rumi Ohgaito<sup>1</sup>, Akinori Ito<sup>1</sup>, Akira Oka<sup>2</sup>

<sup>1</sup>Japan Agency for Marine-Earth Science and Technology, Yokohama, Japan

<sup>2</sup>Atmospheric and Ocean Research Institute, The University of Tokyo, Kashiwa, Japan

Corresponding author: A. Yamamoto (akitomo@jamstec.go.jp)

## Abstract

Increased accumulation of respired carbon in the deep ocean associated with enhanced efficiency of the biological carbon pump is thought to be a key mechanism of glacial CO<sub>2</sub> drawdown. Despite greater oxygen solubility due to seawater cooling, recent quantitative and qualitative proxy data show glacial deep-water deoxygenation, reflecting increased respired carbon accumulation. However, the mechanisms of deep-water deoxygenation and contribution from the biological pump to glacial CO<sub>2</sub> drawdown have remained unclear. In this study, we report the significance of iron fertilization from glaciogenic dust in glacial CO<sub>2</sub> decrease and deep-water deoxygenation using our numerical simulation, which successfully reproduces the magnitude and large-scale pattern of the observed oxygen changes from the present to the Last Glacial Maximum. Sensitivity experiments show that physical changes contribute to only one-half of all glacial deep deoxygenation, whereas the other one-half is driven by iron fertilization and an increase in the whole ocean nutrient inventory. We found that iron input from glaciogenic dust with higher iron solubility is the most significant factor in enhancing the biological pump and deep-water deoxygenation. Glacial deep-water deoxygenation expands the hypoxic waters in the deep Pacific and Indian oceans. The simulated global volume of hypoxic waters is nearly double the present value, suggesting that glacial deep-water was a more severe environment for benthic animals than that of the modern oceans. Our model underestimated the deoxygenation in the deep Southern Ocean because of enhanced ventilation. The model-proxy comparison of oxygen change suggests that a stratified Southern Ocean is required for reproducing the oxygen decrease in the deep Southern Ocean. Iron fertilization and a global nutrient increase contribute to a decrease in glacial CO<sub>2</sub> of more than 30 ppm, which is supported by the model-proxy agreement

削除: Ocedn

削除: surface

削除: accumulation of

削除:

削除: for

削除: reveal

削除: (e.g., more sluggish ocean circulation)

削除: ,

削除: enhanced efficiency of the biological pump

削除: the

削除: for

削除: ement of

削除: O

削除: which

削除: the

削除: is sever environment

削除: the

削除: due to

削除: the

削除: line

削除: Enhanced efficiency of biological pump

削除: s

削除: of

削除: by

50 of oxygen change. Our findings confirm the significance of the biological pump in glacial CO<sub>2</sub> drawdown and  
51 deoxygenation.

52

删除:

54 **1 Introduction**

55 The oceanic carbon cycle has been proposed as a driver of glacial–interglacial CO<sub>2</sub> change; however, the magnitude of glacial  
56 CO<sub>2</sub> reduction of 80–100 ppm has yet to be fully reproduced by numerical model simulations using both an ocean general  
57 circulation model (OGCM) and a biogeochemical model (Ciais et al., 2013). The oceanic **soft-tissue** biological pump, by which  
58 the photosynthetic production, sinking, and remineralization of organic matter store dissolved inorganic carbon in the deep  
59 ocean, is **among** the mechanisms controlling glacial–interglacial as well as future atmospheric CO<sub>2</sub> change (Sarmiento and  
60 Gruber 2006; Sigman et al., 2010; Yamamoto et al., 2018). During glacial periods, the efficiency of the biological pump would  
61 have been enhanced by biogeochemical processes (e.g. dust-borne iron fertilization (Martin, 1990) and **an** increase in nutrient  
62 inventory associated with **a** sea-level drop (Broecker, 1982; Wallmann et al., 2016)) and thus atmospheric CO<sub>2</sub> would have  
63 been transported to the glacial deep ocean. Although changes in marine productivity during glacial periods and its relationship  
64 to the dust deposition flux have been widely supported by proxy records (Kohfeld et al., 2005; Jaccard et al., 2013), there **are**  
65 no direct proxy records of **the** greater accumulation of respired organic carbon. Thus, the contribution of the biological pump  
66 **to** glacial CO<sub>2</sub> reduction is poorly understood.

67  
68 Because the dissolved oxygen cycle is the mirror image of the biological carbon cycle (oxygen is produced by photosynthesis  
69 and is utilized with consistent stoichiometry through the remineralization of sinking organic matter in the ocean interior),  
70 oxygen is consumed in the ocean interior when respired organic carbon **accumulates** in seawater. Thus, reconstructed oxygen  
71 change is useful **to** constrain the biological pump **magnitude** and respired carbon **accumulation**. Proxy data show that, despite  
72 greater oxygen solubility due to lower sea surface temperatures (SSTs), oxygen concentrations decreased throughout the deep  
73 ocean during the Last Glacial Maximum (LGM) (Jaccard and Galbraith, 2012). This indicates greater oxygen consumption  
74 and respired carbon **accumulation**, which could have been caused by several processes **including** greater organic matter  
75 **transport** into the deep ocean, **increasingly** restricted air-sea exchange due to sea-ice expansion, and/or more sluggish ocean  
76 circulation. However, previous modeling studies **have shown** conflicting oxygen changes in LGM simulations (Galbraith and  
77 Jaccard, 2015; **Schmittner and Somes, 2016**; Buchanan et al., 2016; Bopp et al., 2017; **Somes et al., 2017**; Galbraith and de  
78 Lavergne, 2018) and the causes of **the** oxygen **decrease** in the deep ocean have not yet been fully explored.

删除: carbon

删除: one of

删除: CO<sub>2</sub> change,

删除: the

删除: ,

删除: ,

删除: the

删除: were

删除: on

删除: is

删除: d

删除: to the

删除: for

删除: ing

删除: the magnitude of

删除: accumulation of

删除: accumulation of

删除: :

删除: transport of

删除: more

删除: display

删除: the

删除: ,

删除: line

03

04 Furthermore, because most observations provide only qualitative estimates of oxygen changes, previous model-proxy  
 05 comparisons have only discussed the glacial oxygen trend (oxygenation in the upper ocean and deoxygenation in the deep  
 06 ocean). Several recent studies using  $\delta^{13}\text{C}$  in benthic foraminiferal or iodine-to-calcium ratios in planktonic foraminifera were  
 07 able to quantify oxygen concentration changes (Schmiedl and Mackensen, 2006; Hoogakker et al., 2015, 2018; Gottschalk et  
 08 al., 2016; Lu et al., 2016; Bunzel et al., 2017; Umling and Thunell, 2018). These quantitative proxy data provide firmer  
 09 constraints on respired carbon accumulation, such that a quantitative model-proxy comparison of oxygen change is very useful  
 10 for quantifying the contribution of the biological pump to glacial  $\text{CO}_2$  drawdown.

- 删除: only
- 删除: ,
- 删除: changes in
- 删除: Umling and Thunell, 2018;
- 删除: Schmiedl and Mackensen, 2006
- 删除: accumulation of

11

12 In this study, to quantify the impact of changes in the biological pump on glacial carbon and oxygen cycles, we conducted pre-  
 13 industrial (PI) and LGM simulations using the coupled atmosphere–ocean general circulation model (Oka et al., 2011), aerosol  
 14 model (Ohgaito et al., 2018), and ocean biogeochemical model (Yamamoto et al., 2015). We focused here on the iron  
 15 fertilization process in enhancing the biological pump. We attempted to separately quantify iron fertilization effects from desert  
 16 dust and glaciogenic dust (derived from glacier erosion). Previous studies using mineral aerosol models suggest that  
 17 glaciogenic dust significantly contributed to an increase in the dust deposition flux at high latitudes during the LGM (e.g., the  
 18 glaciogenic dust derived from Patagonian glaciers increased dust deposition in the Southern Ocean (SO)) and provided a LGM  
 19 dust deposition flux distribution more consistent with the reported measurements (Mahowald et al., 2006; Ohgaito et al., 2018).  
 20 Moreover, the iron solubility in glaciogenic dust (~3%) is much higher than that in desert dust (~1%) (Schroth et al., 2009);  
 21 however, the higher solubility effect of glaciogenic dust on iron fertilization was not considered in previous modeling studies.  
 22 Glaciogenic dust is a significant source of bioavailable iron (Shoenfelt et al., 2018) and would therefore have a major impact  
 23 on biological productivity in high nutrient and low chlorophyll (HNLC) regions where biological productivity is limited by  
 24 the lack of iron. We also considered the effect of an increase in macronutrients inventory associated with a glacial sea level  
 25 drop of ~120 m (Broecker, 1982; Wallmann et al., 2016). A decrease in the area of continental margins reduced the burial of  
 26 organic matter in margin sediments, leading to increases in the global inventory of phosphate ( $\text{PO}_4$ ) and nitrate ( $\text{NO}_3$ ). Based  
 27 on a recent simulation, increases in  $\text{NO}_3$  and  $\text{PO}_4$  inventories by 15% can be assumed (Wallmann et al., 2016).

- 删除: the
- 删除: for
- 删除: Our new
- 删除: is
- 删除: , separately
- 删除: s
- 删除: ,
- 删除: s
- 删除: s
- 删除: solubility of
- 删除: ,
- 删除: but
- 删除: the
- 删除: supply
- 删除: significantly
- 删除: large
- 删除: D
- 删除: s
- 删除: thus
- 删除: are

54

55 We performed several sensitivity experiments as listed in Table 1 to explore the contribution of changes in atmospheric dust  
56 and nutrient inventory on glacial carbon and oxygen cycles. Moreover, our modeled oxygen changes were compared to recently  
57 reported qualitative (Jaccard and Galbraith, 2012) and quantitative reconstructions (Schmiedl and Mackensen, 2006;  
58 Hoogakker et al., 2015, 2018; Gottschalk et al., 2016; Lu et al., 2016; Bunzel et al., 2017; Umling and Thunell, 2018) to  
59 evaluate the simulated accumulation of respired carbon. Our simulation shows that glaciogenic dust and increased nutrient  
60 inventory play a crucial role in glacial CO<sub>2</sub> decrease and deep-water deoxygenation.

61

## 62 2 Model and experiments

63 The ocean biogeochemical cycle was calculated using the Model for Interdisciplinary Research on Climate (MIROC)-based  
64 offline biogeochemical model, based on Yamamoto et al. (2015), with the implementation of an iron cycle. A one box  
65 atmosphere is coupled to an offline biogeochemical model to predict atmospheric CO<sub>2</sub> concentration through gas exchange  
66 between the atmosphere and ocean surface. For the tracer calculation, the model uses prescribed monthly output data of  
67 horizontal ocean velocities, vertical diffusivity, temperature, salinity, sea surface height, sea surface wind speed, sea-ice  
68 fraction, and sea surface solar radiation, derived from PI and LGM simulations conducted by Oka et al. (2011) using the MIROC  
69 4m AOGCM. Both PI and LGM simulations follow the PMIP2 protocol (Braconnot et al., 2007). MIROC 4m simulates the  
70 weaker and shallower Atlantic Meridional Overturning Circulation (AMOC) during the LGM (see Fig. 1 in Oka et al. (2011)),  
71 which is consistent with δ<sup>13</sup>C distributions reported from proxy data (Curry and Oppo, 2005). The horizontal and vertical  
72 resolutions of the offline biogeochemical model are the same as those in MIROC 4m.

73

74 This biogeochemical model includes two phytoplankton classes (nitrogen fixers and other phytoplankton), zooplankton,  
75 particulate detritus, nitrate (NO<sub>3</sub>), phosphate (PO<sub>4</sub>), dissolved iron (DFe), dissolved oxygen (O<sub>2</sub>), dissolved inorganic carbon  
76 (DIC), alkalinity (ALK), two carbon isotopes (<sup>13</sup>C and <sup>14</sup>C), and an ideal age tracer. The ideal age is set to zero at the surface  
77 and ages at a rate of 1 yr yr<sup>-1</sup> in the ocean interior. Constant stoichiometry relates the C, N, P, and DFe content of the biological  
78 variables and their exchanges to inorganic variables (NO<sub>3</sub>, PO<sub>4</sub>, DFe, O<sub>2</sub>, ALK, and DIC). The maximum phytoplankton growth

删除: are

删除: ; Schmiedl and Mackensen, 2006

删除: enhanced efficiency of biological pump associated with

删除: s

删除: the

删除: by

删除: in order

删除: ,

删除: at

88 and microbial remineralization rates are assumed to increase with seawater temperature (Eppley, 1972). The iron cycle that is  
89 incorporated in the biogeochemical model mainly follows Parekh et al. (2005). In addition to dust deposition, which is assumed  
90 as the only DFe source in Parekh et al. (2005), sedimentary, and hydrothermal DFe inputs are considered. When the DFe  
91 concentration exceeds the total ligand concentration, a formulation for the DFe scavenging rate of Moore and Braucher (2008)  
92 is applied. To obtain a realistic distribution of the iron-limited region, total ligand concentration, which controls the amount of  
93 the free form of iron, is set to a global constant value of  $0.6 \mu\text{mol m}^{-3}$  instead of the original value of  $1 \mu\text{mol m}^{-3}$  (Fig. 1a).

94  
95 Dust deposition flux is obtained from the monthly output data of MIROC-ESM in the PI and LGM simulations (Ohgaito et al.,  
96 2018). Dust is assumed to contain a constant fraction of iron (3.5 wt%). 1% of the iron in desert dust is assumed to  
97 instantaneously dissolve at the sea surface. The global DFe flux from dust in the PI is  $2.7 \text{ Gmol yr}^{-1}$  (Table 1). We used two  
98 sets of LGM dust deposition flux labelled as LGM<sub>ctl</sub> and LGM<sub>glac</sub> as calculated in a previous study (Ohgaito et al., 2018).  
99 LGM<sub>ctl</sub> is the standard LGM simulation, which has been submitted to Coupled Model Intercomparison Project Phase 5 /  
00 Paleoclimate Modelling Intercomparison Project (CMIP5/PMIP4). LGM<sub>glac</sub> is identical to LGM<sub>ctl</sub>, except that an additional  
01 glaciogenic dust flux based on Mahowald et al. (2006) is included. In LGM<sub>ctl</sub>, the dust deposition flux is underestimated in  
02 North America, Eurasia, the South Pacific, the SO, and Antarctica compared to the proxy data of ice and sediment cores  
03 (Kohfeld et al., 2013; Albani et al., 2014). Because glaciogenic dust increases dust deposition at high latitudes, the  
04 underestimation is generally improved in LGM<sub>glac</sub> (see Ohgaito et al., 2018, for more details). The global DFe fluxes from  
05 dust are  $8.6 \text{ Gmol yr}^{-1}$  and  $13.9 \text{ Gmol yr}^{-1}$  for LGM<sub>ctl</sub> and LGM<sub>glac</sub>, respectively.

06  
07 Present observation generally shows a lower Fe solubility at a higher Fe concentration in aerosols and a higher solubility at a  
08 lower concentration (Fig. S1). A wider range of aerosol Fe solubility (from 0.2% to 48%) has been derived from observations  
09 over the SO, but different types of Fe-containing minerals such as pyrogenic Fe oxides can be considered to achieve high Fe  
10 solubilities (Ito et al., 2019). Thus, an assumed constant iron solubility of 2% in all types of dust could lead to overestimation  
11 of a total DFe flux from different types of Fe-containing aerosols during the LGM (Muglia et al., 2017). However, a much  
12 higher Fe solubility (1–42% of Fe solubility) as derived from observations for the LGM aerosols in Antarctica has suggested

删除: D

删除: fluxes,

删除: fluxes

删除: as DFe sources

删除:

删除: , and

删除: instantaneously

删除: that were

删除: was

删除: Since

23 that an assumed constant iron solubility of 1–2% for all types of dust could lead to a DFe flux underestimation during the LGM  
24 (Conway et al., 2015). In LGM\_glac3%, an iron solubility of 3% in glaciogenic dust is assumed (Schroth et al., 2009), such  
25 that the global DFe flux is 24.5 Gmol yr<sup>-1</sup>. This value is approximately 10 times larger than that of the PI simulation and is  
26 larger than a recent estimation, suggesting that a quadrupling of the global DFe flux is constrained by a model-proxy  
27 comparison of δ<sup>15</sup>N and δ<sup>13</sup>C (Muglia et al., 2018). As with the present DFe input from dust, glacial DFe input has large  
28 uncertainties. As an upper estimate of the DFe flux from dust, we set the iron solubility at 10% in glaciogenic dust in  
29 LGM\_glac10%.  
30  
31 The DFe input flux from the sediments is estimated based on Moore and Braucher (2008). We assumed that the sedimentary  
32 DFe flux is proportional to the flux of organic carbon reaching the sea floor. To consider the realistic bathymetry of the  
33 continental shelves, the iron flux is weighted by the fraction of bottom area of the ETOPOV2 data that falls within the bounds  
34 of the model grid cell. The global DFe flux from the sediments in the PI is 33.1 Gmol yr<sup>-1</sup>. In the LGM simulations, the DFe  
35 input from sedimentary sources changes according to the flux of organic carbon reaching the sea floor. A decrease in the DFe  
36 input from sedimentary sources because of a sea-level drop is not considered. Muglia et al. (2017) showed this effect causes a  
37 CO<sub>2</sub> increase of 15 ppm. The hydrothermal DFe flux is regulated by the ridge spreading rate, as parameterized by a constant  
38 DFe/Helium ratio (Tagliabue et al., 2010). The hydrothermal DFe flux in the PI is ~8.5 Gmol yr<sup>-1</sup>. In the LGM simulations,  
39 the DFe input from hydrothermal sources is the same as that from PI.  
40  
41 The biogeochemical model was initialized from annual mean climatology data based on the World Ocean Atlas 2009  
42 (WOA2009: Garcia et al., 2010a and 2010b) for dissolved NO<sub>3</sub>, PO<sub>4</sub>, and O<sub>2</sub> and the Global Ocean Data Analysis Project (Key  
43 et al., 2004) for DIC and ALK. The initial DFe concentration is a constant value of 0.6 nM. For the spin-up, the last 50 years  
44 of data in the MIROC PI experiments were cyclically applied to the offline ocean biogeochemical model. The model was spun  
45 up for more than 3000 years with a prescribed atmospheric CO<sub>2</sub> concentration of 285 ppm to eliminate model drift in the global  
46 inventory of all tracers. Similar to Yamamoto et al. (2015), all physical and biogeochemical tracers, except salinity and

删除: so

删除: Thus, a

删除: of

删除: This assumption is consistent with ice core data of EPICA Dome C from East Antarctica (Conway et al., 2015).

删除: In present days, wider range of aerosol Fe solubility (from 0.2% to 48%) has been derived from observations over the Southern Ocean, but different types of Fe-containing minerals such as pyrogenic Fe oxides could be considered to achieve the high Fe solubilities (Ito et al., 2019).<sup>4</sup>

删除: In order t

删除: due to

删除: not changed

删除: the

删除: concentration of

删除: a

删除: in order

64 dissolved iron, have correlation coefficients with observational data greater than 0.85 and normalized standard deviation values  
65 between 0.7 and 1.1.

66

67 LGM experiments were run for 3000 years, following 3000 years of spin-up under PI conditions. The atmospheric CO<sub>2</sub>  
68 concentration was predicted. We increased the salinity, PO<sub>4</sub>, and NO<sub>3</sub> inventory by 3% to account for the reduced ocean  
69 volume because of the sea level drop. All experiments are listed in Table 1. LGM\_clim uses LGM boundary conditions.  
70 LGM\_dust is based on LGM\_clim but uses the dust deposition flux of LGMctl. Similarly, LGM\_glac3% and LGM\_glac10%  
71 use the dust deposition flux of LGMglac, but with an iron solubility of glaciogenic dust of 3% and 10%, respectively. LGM\_all  
72 is similar to LGM\_glac3%, but the NO<sub>3</sub> and PO<sub>4</sub> inventories are increased by 15%. This assumption is based on a recent model  
73 simulation that shows a ~15% increase in nutrient inventory is caused by reduced organic matter burial in shallow sediments  
74 associated with a sea level drop (Wallmann et al., 2016). In our simulations, changes in benthic denitrification were not  
75 considered. Some et al. (2017) show that a decrease in benthic denitrification because of a sea level drop reduces NO<sub>3</sub> loss  
76 and thus leads to a larger NO<sub>3</sub> inventory in the LGM ocean. We analyzed the results from the last 100 years of each simulation.

77

### 78 3 Results and Discussion

#### 79 3.1 Glacial nutrient cycles and export production

80 In the LGM\_clim, which uses LGM climate boundary conditions, the NO<sub>3</sub> redistribution induced by weaker and shallower  
81 AMOC reduces nutrient supply from the deep ocean to the surface (Table 2 and Fig. 2). The NO<sub>3</sub> concentration in the euphotic  
82 zone decreases by 12% and the global export production (EP) is reduced by 0.54 Pg C yr<sup>-1</sup> compared to that of the PI simulation.  
83 Corresponding to the surface NO<sub>3</sub> decrease, significant EP decreases are found in the North Atlantic and North Pacific (Fig.  
84 3a and Fig. S2). However, the surface DFe concentration slightly changes. Because these changes in DFe and NO<sub>3</sub> decrease  
85 the iron-limited areas by 27% (Fig. 1b), the simulated LGM climate tends to mitigate the impacts of iron fertilization on  
86 biological productivity and the carbon cycle.

87

删除: of more

删除: A

删除: is

删除: in the first year of simulations

删除: due to

删除: s

删除: burial of

删除: redistribution of

删除: Atlantic meridional overturning circulation (

删除: )

删除: ,

删除: with

删除: 1

删除: On the other hand

删除: dissolved iron (

删除: )

删除: slightly

删除: Since

删除: shrink

07 To evaluate the impacts of desert and glaciogenic dust on the ocean biogeochemical cycles, we conducted sensitivity studies.  
 08 The DFe input from desert dust with a 1% iron solubility was applied in LGM\_dust, whereas glaciogenic dust with 3% or 10%  
 09 iron solubility was additionally applied in LGM\_glac3% or LGM\_glac10%, respectively. Iron fertilization from only desert  
 10 dust has a limited impact on the EP. Iron fertilization from both desert and glaciogenic dust increases the EP by 0.88 Pg C yr<sup>-1</sup>  
 11 south of 45°S, whereas the EP decreases by 0.86 Pg C yr<sup>-1</sup> north of 45°S, where most oceans are nitrogen-limited regions  
 12 (LGM\_glac3% – LGM\_clim; Table 2). Enhanced primary production consumes the NO<sub>3</sub> of the euphotic zone in the SO and  
 13 its anomaly is transported to the Antarctic bottom water (AABW). Subsequently, the surface NO<sub>3</sub> reduction in the SO is also  
 14 transported to low-latitude regions via surface and intermediate waters (Fig. 2), thus reducing the EP in nitrogen-limited regions  
 15 at low latitudes. Remarkable EP reductions occur north of the iron-limited regions of the SO (Fig. 3b). Our results demonstrate  
 16 that enhanced biotic carbon export in the SO is partly compensated for by reduced carbon export in low-latitude regions. From  
 17 the comparison between the effect of desert dust (LGM\_dust – LGM\_clim) and that of glaciogenic dust (LGM\_glac3% –  
 18 LGM\_dust), we found that an increase in the EP due to dust-bone iron fertilization in the SO is mainly caused by glaciogenic  
 19 dust (Table 2).

20  
 21 For 15% increases in NO<sub>3</sub> and PO<sub>4</sub> inventory associated with sea level drop (LGM all), the EP increases, globally in the  
 22 nitrogen-limited regions, leading to a global EP increase of 0.86 Pg C yr<sup>-1</sup> (LGM\_all – LGM\_glac3%; Table 2). Simulated EP  
 23 changes from the PI are in good agreement with the paleoproductivity reconstruction (Kohfeld et al., 2013) (Fig. 3c). Among  
 24 the common patterns is the north-south dipole pattern in the SO with an EP decrease at higher latitudes and an EP increase at  
 25 lower latitudes. The EP decrease at higher latitudes is attributed to sea ice expansion and the associated reduction of surface  
 26 shortwave radiation (Oka et al., 2011), whereas iron fertilization increases the EP at lower latitudes. In the model, the EP  
 27 changes also have an east-west dipole pattern; slight EP increases are found in the South Pacific Ocean and significant EP  
 28 increases occur in the South Atlantic and Indian oceans. We found that this pattern is attributed to iron fertilization by  
 29 glaciogenic dust. Glaciogenic dust derived from Patagonian glaciers is transported to the South Atlantic and Indian oceans by  
 30 the southern westerly wind; however, it is unable to reach the South Pacific (Fig. S3). Proxy data show no clear east-west  
 31 dipole pattern, suggesting that the model underestimates iron fertilization in the Pacific sector of the Southern Ocean. However,

- 删除: is
- 删除: is
- 删除: ve
- 删除: because dust deposition flux of the Southern Ocean is underestimated in LGM\_dust
- 删除: in the
- 删除: with iron limitation,
- 删除: in the
- 删除: reduction of
- 删除: the
- 删除: in the
- 删除: the
- 删除: export production
- 删除: Under
- 删除: is
- 删除: d
- 删除: by
- 删除: 2005
- 删除: One of
- 删除: decrease of
- 删除: -
- 删除: increase of
- 删除: -
- 删除: the expansion of
- 删除: ,
- 删除: On the other hand
- 删除: both the proxy data and model show no significant changes
- 删除: of EP
- 删除: clear
- 删除: O
- 删除: O
- 删除: , but
- 删除: 2

65 proxy data in the South Pacific remain sparse and a quantitative comparison of EP changes between the South Atlantic and  
66 South Pacific is limited. Therefore, further proxy data in the South Pacific is required for a comprehensive understanding of  
67 the glacial EP changes and iron fertilization.

删除: The realistic distribution of glaciogenic dust deposition simulated by an aerosol model and our consideration of its higher iron solubility enable us to reproduce the east-west dipole pattern of EP changes

### 69 3.2 CO<sub>2</sub> reduction and its relationship to efficiency of the biological pump and dust flux

70 Climate change reduces the atmospheric CO<sub>2</sub> concentration by 26.4 ppm (LGM\_clim – PI, Table 2), which is similar to that  
71 of previous simulations (Chikamoto et al, 2012; Menviel et al., 2012; Kobayashi et al., 2015). Circulation changes (i.e. a  
72 weaker and shallower AMOC and AABW expansion) cause DIC to decrease in the upper ocean and increase below 2000 m  
73 depth, such that the vertical DIC gradient between the surface and deep oceans is enhanced (Fig. 4). The efficiency of the  
74 oceanic biological pump is calculated following Ito and Follows (2005). The global mean preformed PO<sub>4</sub> is the difference  
75 between the total globally averaged PO<sub>4</sub> and global mean remineralized PO<sub>4</sub>,  $P_{pref} = P_{tot} - P_{remi}$ . Here,  $P_{pref}$  is the preformed  
76 PO<sub>4</sub> concentration,  $P_{tot}$  is the total PO<sub>4</sub> concentration, and  $P_{remi}$  is the remineralized PO<sub>4</sub> concentration. The remineralized PO<sub>4</sub>  
77 is given by  $P_{remi} = AOU \times R_{P:O}$ , where  $R_{P:O}$  is a constant phosphorous to oxygen ratio, and AOU is apparent oxygen utilization.  
78 A decrease in preformed PO<sub>4</sub> and thus an increase in remineralized PO<sub>4</sub> indicate an increase in the efficiency of the oceanic  
79 biological pump. Although globally integrated EP decreases, circulation change and deepening of the remineralization profile  
80 due to seawater cooling (Matsumoto, 2007) reduce the preformed nutrient inventory, enhancing the efficiency of the biological  
81 pump (Table 2). The enhanced accumulation of respired carbon associated with the more efficient biological pump and  
82 increased CO<sub>2</sub> solubility from the lower SST contribute to a decreased CO<sub>2</sub>. Notably, the AOU is different from true oxygen  
83 utilization due to the air-sea disequilibrium which is on the order of 20 mmol m<sup>-3</sup> in deep-water formation regions (Russell  
84 and Dickson, 2003; Duteil et al., 2013). Changes in surface ocean disequilibrium between the PI and LGM simulations might  
85 lead to large errors in the AOU changes.

删除: ,

删除: expansion of

删除: dissolved inorganic carbon (

删除: )

删除: o

删除: G

删除: D

删除: the

删除: and thus

删除: e

删除: a

87 Iron fertilization from desert and glaciogenic dust enhances the vertical DIC gradient and causes a CO<sub>2</sub> reduction of 1.2 ppm  
88 (LGM\_dust – LGM\_clim) and 15.6 ppm (LGM\_glac3% – LGM\_dust), respectively. Our results show that the glacial CO<sub>2</sub>  
89 reduction due to dust-bone iron fertilization is mainly driven by glaciogenic dust. A simulated total CO<sub>2</sub> reduction of 16.8 ppm

删除: dust

删除: S

07 induced by iron fertilization is within the range of previous studies using OGCM or Earth system Models of Intermediate  
08 Complexity (EMICs) (8-25 ppm CO<sub>2</sub> drawdown (Bopp et al., 2003; Parekh et al., 2006; Tagliabue et al., 2009; Oka et al.,  
09 2011; Menziel et al., 2012; Lambert et al., 2015; Heinze et al., 2016; Muglia et al., 2017). DFe supply from dust also contributes  
10 to the glacial CO<sub>2</sub> reduction through enhanced efficiency of the biological pump (Table 2). The simulated atmospheric CO<sub>2</sub>  
11 concentration is proportionally reduced to the preformed PO<sub>4</sub> (Fig. 5a), similar to previous simulations under the present  
12 climate (Ito and Follows, 2005; Marinov et al., 2008). Figure 5b shows the CO<sub>2</sub> change in response to the DFe input magnitude.  
13 The iron fertilization efficiency to reduce CO<sub>2</sub> decreases with increasing DFe flux. This nonlinear response is driven by a  
14 decrease in the iron-limited areas and the associated weakening of the iron fertilization effect on EP (Fig. 5c). Because the  
15 iron-limited region dramatically decreases in size and the CO<sub>2</sub> difference between LGM\_glac3% and LGM\_glac10% is small,  
16 the CO<sub>2</sub> reduction of 20 ppm in LGM\_glac10% is near the upper limit (i.e., there are no iron-limited regions and thus no  
17 additional CO<sub>2</sub> reduction).

删除: ing the

删除: reduced

删除: magnitude of

删除: efficiency of

删除: effect of

删除: Since

删除: shrinks

删除: close to

删除: ,

18  
19 The simulated upper limit of CO<sub>2</sub> reduction resulting from iron fertilization is not a robust result because present iron models  
20 have large uncertainty. While Parekh et al. (2008) show an upper limit of 10 ppm, other simulations show CO<sub>2</sub> decrease by  
21 greater than 20 ppm (Oka et al., 2011; Muglia et al., 2017). To obtain a better understanding of the impact of iron fertilization  
22 on glacial CO<sub>2</sub> decrease, the variability of the upper limit among iron models should be investigated in a future study.

23  
24 Increases in nutrient inventory from lower sea levels drive an additional CO<sub>2</sub> drawdown by 16 ppm (LGM\_all – LGM\_glac3%).  
25 We found that changes in the biological pump induced by iron fertilization and an increase in nutrient inventory contribute to  
26 a glacial CO<sub>2</sub> decrease of greater than 30 ppm. The resultant total CO<sub>2</sub> reduction is ~60 ppm, which our model does not  
27 reproduce as the full variation in the glacial-interglacial CO<sub>2</sub> change. Note that changes in the sedimentation process (i.e.,  
28 carbonate compensation and burial-nutrient feedback) are, not considered in our simulation. The simulated increase in the  
29 bottom water DIC (Fig. 4) would enhance calcium carbonate dissolution in the sediments and thereby increase ocean alkalinity,  
30 leading to a further CO<sub>2</sub> decrease (Bouttes et al., 2011; Brovkin et al., 2012; Kobayashi et al., 2018). The long-term balance  
31 between the burial of organic material and nutrient input through weathering is also potentially important for the response in

删除: line by more

删除: resulting

删除: of

删除: the

删除: process is

删除: dissolution of

删除: decline

48 atmospheric CO<sub>2</sub> and related tracers to changes in ocean biological cycles (Roth et al., 2014; Wallmann et al., 2016). For  
49 example, Tschumi et al. (2011) show that the nutrient-burial feedback significantly amplifies the effect of an increase in the  
50 PO<sub>4</sub> inventory on the glacial CO<sub>2</sub> decrease. Menviel et al. (2012) quantified the implication of ocean-sediment-lithosphere  
51 coupling for factorial experiments with an altered iron fertilization and altered PO<sub>4</sub> inventory from transient glacial-interglacial  
52 simulations. Considering that EP increases due to iron fertilization and the nutrient increase is smaller in our simulations than  
53 that in previous studies (Tschumi et al., 2011; Menviel et al., 2012), the effect of burial-nutrient feedback on the glacial CO<sub>2</sub>  
54 reduction may be smaller than previously estimated. As described in the next section, to assess the simulated accumulation of  
55 respired carbon, we compared the simulated oxygen changes to qualitative and quantitative proxy records.

删除: In

删除: with

56

### 57 3.3 Model-proxy comparison of glacial oxygen changes

58 Compared to the compilation of qualitative and quantitative proxy records of oxygen change from the Holocene to Last Glacial  
59 Maximum, LGM\_clim shows an increase in oxygen for the entire SO and underestimates deoxygenation in the deep Pacific  
60 and Indian oceans, in contrast to the proxy records (Fig. 6a). However, LGM\_all successfully reproduces large-scale spatial  
61 patterns of oxygen change, including for the SO (Fig. 6b). Moreover, the simulated changes in oxygen concentration agree  
62 well with quantitative reconstructions: a 45-65 mmol m<sup>-3</sup> decrease in the deep North Atlantic (Hoogakker et al., 2015), an ~30-  
63 80 mmol m<sup>-3</sup> decrease in the eastern equatorial Pacific (Hoogakker et al., 2018; Umling and Thunell, 2018), and a >80 mmol  
64 m<sup>-3</sup> in the upper SO of the Pacific sector (Lu et al., 2016). Our results clearly show the importance of iron fertilization and an  
65 increase in nutrient inventory in global deep deoxygenation. These model-proxy agreements of oxygen change support the  
66 simulated CO<sub>2</sub> decrease of 30 ppm by the biological pump. However, the reconstructed O<sub>2</sub> decrease of ~175 mmol m<sup>-3</sup> in the  
67 deep SO (Gottschalk et al., 2016) is much greater than the simulated decrease of ~30 mmol m<sup>-3</sup> from LGM\_all; thus, the  
68 respired carbon accumulation in the deep SO is underestimated in our model. This may be one of the reasons why the glacial-  
69 interglacial CO<sub>2</sub> change of ~100 ppm cannot be reproduced in our simulations.

删除: with

删除: the

删除: O

删除: which is

删除: On the other hand

删除: are in good agreement

删除: the enhanced biological pump associated with

删除: for

删除: larger

删除: ,

删除: which

删除: means that the accumulation of

删除: is the one

70

71 To clarify the mechanism of O<sub>2</sub> change from LGM\_all – PI, we decomposed the O<sub>2</sub> change into changes in saturation (O<sub>2sat</sub>)  
72 and apparent oxygen utilization (AOU), where  $\Delta O_2 = \Delta O_{2sat} - \Delta AOU$ . O<sub>2sat</sub> is computed from simulated seawater temperature

删除: h

删除: The

90 and salinity, and AOU by subtracting the O<sub>2</sub> concentration from O<sub>2sat</sub>. Ocean cooling increases O<sub>2sat</sub> globally, increasing the  
91 global mean value by 25.5 mmol m<sup>-3</sup> (Fig. 7a). As with the O<sub>2</sub> change, ΔAOU shows a contrast between the upper and deep  
92 oceans (Fig. 7b). At a depth of 0-800 m, the AOU decreases by 5.2 mmol m<sup>-3</sup> north of 45°S, which results from the decrease  
93 in biological oxygen consumption associated with EP reduction and increased ventilation (Fig. 7f). Therefore, the combined  
94 effects of an O<sub>2sat</sub> increase and AOU decrease contribute to an overall O<sub>2</sub> increase in the upper ocean. In the deep ocean (>2  
95 km depth), the sum of AOU increases by 72.8 mmol m<sup>-3</sup> (LGM\_all in Table 2), overcoming the O<sub>2sat</sub> increase, resulting in  
96 deep O<sub>2</sub> depletion. The relationship between changes in the O<sub>2</sub> concentration, O<sub>2sat</sub>, and AOU are consistent with that of a  
97 previous simulation (Bopp et al., 2017).

98  
99 The ΔAOU is also decomposed into effects of climate change (LGM\_clim – PI), iron fertilization (LGM\_glac3% – LGM\_clim)  
100 and an increase in nutrient inventory (LGM\_all – LGM\_glac3%). The effects of climate change, circulation change, restricted  
101 air-sea gas exchange from sea-ice expansion, and deepening of remineralization due to seawater cooling leads to the AOU  
102 increasing by 37.3 mmol m<sup>-3</sup> in the deep ocean (Table 2). In the deep North Atlantic, the simulated water mass age is older in  
103 the LGM than in the PI by up to 500 years, suggesting reduced ventilation (Fig. 7f). Therefore, significant AOU increases  
104 occur (Fig. 7c). Meanwhile, in the SO and deep Pacific Ocean, an increase in ventilation tends to decrease the AOU and thus  
105 partly compensates for the increase in the AOU. Regarding the effects of iron fertilization and nutrient inventory, the EP  
106 changes associated with iron fertilization and an increase in nutrient inventory enhance biological oxygen consumption and  
107 thus increase the AOU by 21.4 and 14.1 mmol m<sup>-3</sup> in the deep ocean, respectively (Table 2 and Fig. 7d\_e). In particular,  
108 glaciogenic dust causes an increase in the AOU of 19.8 mmol m<sup>-3</sup>. Our results demonstrate that in addition to climate change,  
109 enhanced biological oxygen consumption associated with iron fertilization and increased nutrient inventory are crucial drivers  
110 of glacial deoxygenation in the deep ocean. While some previous modelling studies show deep ocean oxygenation during the  
111 LGM (Buchanan et al., 2016; Galbraith and Laverigne, 2018), this study and others reproduce deep ocean deoxygenation  
112 (Galbraith and Jaccard, 2015; Schmittner and Somes, 2016; Bopp et al., 2017; Somes et al., 2017). The conflicting oxygen  
113 change between the previous simulations can be attributed to different treatments of enhanced biological oxygen consumption

删除: ,

删除: is calculated

删除: the

删除: in

删除: which

删除: es

删除: ,

删除: are found there

删除: cancels out

删除: As for

删除: some other studies

25 because iron fertilization and increased nutrient inventory are not considered in these simulations ~~that~~ fail to reproduce deep  
26 deoxygenation (Buchanan et al., 2016; Galbraith and Lavergne, 2018).

27

28 Glacial oxygen change expands the volume of hypoxic waters (defined here as  $[O_2] < 80 \text{ mmol m}^{-3}$ ) below 1000 m ~~depth~~, ~~such~~,  
29 that the simulated global volume ~~increases~~ from the present value of 120 Mkm<sup>3</sup> to 237 Mkm<sup>3</sup> in LGM ~~all~~. Significant  
30 expansion occurs in the deep Pacific and Indian ~~oceans~~ (Fig. 8), with hypoxic waters also appearing in the upper SO in the  
31 Pacific sector, ~~consistent~~ with proxy records (Hoogakker et al., 2018; Lu et al., 2016). ~~Because~~ hypoxic conditions are lethal  
32 for more than ~~one~~-half of marine benthic animals (Vaquer-Sunyer and Duarte, 2008), expansion of hypoxic water in the deep  
33 ocean ~~can~~ have an adverse impact on benthic fauna. ~~Determining the~~ biotic responses to glacial expansion of hypoxic water  
34 would be helpful for understanding the biotic response to future deoxygenation associated with global warming.

35

36 Finally, we discuss underestimation of deoxygenation in the deep SO in LGM ~~all~~. ~~Because~~ simulated changes in the biological  
37 pump and sea-ice distributions are consistent with reconstructions (Obase et al., 2017), we ~~then addressed circulation~~ ~~changes~~,  
38 The simulated water mass age of the deep SO is younger ~~during~~ the LGM than ~~during~~ the PI by ~200 years (Fig. 7f), indicating  
39 an increase in ventilation. However,  $\Delta^{14}C$  records show an increase in water mass age ~~of~~ more than 1000 years, and thus  
40 increased stratification (Skinner et al., 2010; Burke and Robinson, 2012). Enhanced mixing of surface waters with deep waters  
41 supplies oxygen-rich surface waters ~~to~~ the deep ocean and simultaneously releases carbon accumulated in the deep water to  
42 the atmosphere. Therefore, we attribute the underestimation of deoxygenation and carbon accumulation in ~~the~~ deep SO to  
43 overestimated ventilation. Our results suggest that ~~a~~ stratified SO is required for reproducing glacial CO<sub>2</sub> drawdown and  
44 oxygen decline in the deep SO, ~~consistent~~ with ~~recent~~ paleo-proxy data and models (Fischer et al., 2010; Sigman et al., 2010;  
45 Kobayashi et al., 2015).

46

#### 47 4 Conclusion and remarks

48 We quantified ~~the~~ impacts on glacial deoxygenation and CO<sub>2</sub> decreases caused by glaciogenic dust with higher iron solubility  
49 and increase in nutrient inventory associated with ~~a~~ sea-level drop, using the coupled atmosphere–ocean general circulation

删除: which

删除: o

删除: of hypoxic waters

删除: O

删除: which is

删除: Since

删除: could

删除: The

删除: Since

删除: turn our attention to

删除: in circulation

删除: in

删除: in

删除: by

删除: in

删除: the

删除: which is

删除: the

删除: ; Fischer et al., 2010

删除: y

删除: ,

71 model, aerosol model, and ocean biogeochemical model. As a result, we successfully reproduced the magnitude and large-  
72 scale pattern of the observed oxygen change between the present and LGM. In conclusion, our results show that iron  
73 fertilization from glaciogenic dust and an increase in nutrient inventory are responsible for the glacial CO<sub>2</sub> decline of greater,  
74 than 30 ppm and approximately one-half of deep ocean deoxygenation. These results also demonstrate the usefulness of the  
75 quantitative model-proxy comparison of oxygen change in understanding glacial-interglacial CO<sub>2</sub> change. However, large  
76 uncertainty remains because of the limited number of proxy data of quantitative oxygen change. Thus, we anticipate our  
77 findings will encourage studies to obtain further qualitative and quantitative reconstructions from throughout the global deep  
78 ocean. A comparison between the models and other proxy data (e.g.,  $\delta^{13}\text{C}$ , (Schmittner and Somes, 2016)) is also required to  
79 obtain a more robust and comprehensive understanding of the glacial carbon cycle.

删除: find

删除: the enhanced efficiency of the biological pump

删除: is

删除: more

删除: for

删除: , due to

删除: would

删除: gain

删除: The

删除: ,

80  
81 The changes in nutrient inventory during the LGM have large uncertainties. Previous studies estimate that the oceanic PO<sub>4</sub> and  
82 NO<sub>3</sub> inventories could have been 15–40% (Tamburini and Föllmi, 2009; Wallmann et al., 2016) and 10-100% (Deutsch et al.,  
83 2004; Eugster et al., 2013; Somes et al., 2017) greater during glacial compared to interglacial periods, respectively. Moreover,  
84 Somes et al. (2017) shows that sedimentary  $\delta^{15}\text{N}$  records provide no constrain on this effect. Future simulations should test the  
85 biogeochemical sensitivity to nutrient inventory changes.

86  
87 We focused on the impacts of DFe flux changes from the dust on glacial CO<sub>2</sub> drawdown and deoxygenation in this study.  
88 However, changes in the sedimentary and hydrothermal DFe flux and ligand concentration that are not considered in this study  
89 could also be important. A glacial sea-level drop decreases the sedimentary DFe flux due to the continental shelf reduction,  
90 However, the hydrothermal DFe flux is increased by the lower sea level and bottom pressure (Middleton et al., 2016). Muglia  
91 et al. (2017) show that the changes in sedimentary and hydrothermal DFe flux associated with a sea-level drop increase CO<sub>2</sub>  
92 by 15 ppm and decrease CO<sub>2</sub> by 6 ppm, respectively. Although sedimentary DFe flux is proportional to the organic carbon  
93 flux reaching the seafloor in our model, a parametrization with the Dfe flux as a function of organic carbon flux and bottom  
94 oxygen concentrations is proposed in Dale et al. (2015). Glacial deep-water deoxygenation would increase sedimentary DFe  
95 flux, leading to a further CO<sub>2</sub> decrease via the biological pump. Ligand concentrations strongly control DFe concentrations

删除: changes in

删除: the

删除: be

删除: G

删除: reduction in

删除: ves

删除: On the other hand

删除: through

.14 (Gledhill and Buck, 2012). Because the ligand concentration is affected by numerous factors (Völker and Tagliabue, 2015),  
.15 changes in ligand concentration from the PI to LGM have large uncertainty. Thus, we quantified the effect of DFe flux changes  
.16 under a constant ligand concentration in the PI and LGM simulations. Changes in the sedimentary and hydrothermal DFe flux  
.17 and ligand concentration should be the subject of future research.

删除: y

删除: changes in

.18  
.19 Our model-proxy comparison shows the importance of the combination of a more sluggish SO circulation and enhanced  
.20 biological transport of organic matter in the increased accumulation of respired carbon and deoxygenation in the deep SO.  
.21 However, present climate models cannot reproduce the stratified SO. A possible reason is that they are too coarse to capture  
.22 the process of dense water formation on the Antarctic shelf and tend to underestimate the strength of stratification in the SO  
.23 (Heuzé et al., 2013). The brine rejection process and/or change in the vertical diffusion coefficient could be necessary to  
.24 reproduce the stratified SO (Kobayashi et al., 2015; Bouttes et al., 2011). Similar to glacial oxygen changes, changes in ocean  
.25 circulation in the SO are crucial in projecting future oxygen changes associated with global warming (Yamamoto et al., 2015).

删除: for

删除: greater

删除: the climate models

.26 Therefore, an understanding of glacial oxygen changes will aid in better understanding and predicting future oxygen changes.

删除: for

删除: the

删除: help us to

.27

36 **Acknowledgements**

37 This work was supported by the Integrated Research Program for Advancing Climate Models from the Ministry of  
38 Education, Culture, Sports, Science and Technology, Japan, and JSPS KAKENHI grant number 17H06323. The simulations  
39 with the offline biogeochemical model were performed using the Fujitsu PRIMEHPC FX10 system in the Information  
40 Technology Center, University of Tokyo.

41

42

43 **References**

- 44 Albani, S., Mahowald, N. M., Perry, A. T., Scanza, R. A., Zender, C. S., Heavens, N. G., Maggi, V., Kok, J. F., and Otto-  
45 Bliesner, B. L.: Improved dust representation in the Community Atmosphere Model., *J. Adv. Model. Earth Sy.*, 6,  
46 541–570, <https://doi.org/10.1002/2013ms000279>, 2014.
- 47 Bopp, L., Kohfeld, K. E., and Le Qu'ere, C.: Dust impact on marine biota and atmospheric CO<sub>2</sub> during glacial periods,  
48 *Paleoceanography*, 18, 1046, doi:10.1029/2002PA000810, 2003.
- 49 Bopp, L., Resplandy, L., Orr, J. C., Doney, S. C., Dunne, J. P., Gehlen, M., Halloran, P., Heinze, C., Ilyina, T., Séférian, R.,  
50 Tjiputra, J., and Vichi, M.: Multiple stressors of ocean ecosystems in the 21st century: projections with CMIP5  
51 models, *Biogeosciences*, 10, 6225–6245, <https://doi.org/10.5194/bg-10-6225-2013>, 2013.
- 52 Bopp, L., Resplandy, L., Untersee, A., Le Mezo, P., and Kageyama, M.: Ocean (de)oxygenation from the Last Glacial  
53 Maximum to the twenty-first century: insights from Earth System models, *Philos. T. Roy. Soc. Lond. A*, 375, 2102,  
54 <https://doi.org/10.1098/rsta.2016.0323>, 2017.
- 55 Bouttes, N., Paillard, D., Roche, D. M., Brovkin, V., and Bopp, L.: Last Glacial Maximum CO<sub>2</sub> and <sub>13</sub>C successfully  
56 reconciled, *Geophys. Res. Lett.*, 38, L02705, doi:10.1029/2010gl044499, 2011.
- 57 Braconnot, P., Otto-Bliesner, B., Harrison, S., Joussaume, S., Peterchmitt, J.-Y., Abe-Ouchi, A., Crucifix, M., Driesschaert,  
58 E., Fichefet, Th., Hewitt, C. D., Kageyama, M., Kitoh, A., Laine, A., Loutre, M.-F., Marti, O., Merkel, U., Ramstein,  
59 G., Valdes, P., Weber, S. L., Yu, Y., and Zhao, Y.: Results of PMIP2 coupled simulations of the Mid-Holocene and

60 Last Glacial Maximum – Part 1: experiments and large-scale features, *Clim. Past*, 3, 261–277, doi:10.5194/cp-3-  
61 261-2007, 2007.

62 Broecker, W. S.: Glacial to interglacial changes in ocean chemistry, *Progress in Oceanography*, 11, 151–197,  
63 doi:10.1016/0079-6611(82)90007-6, 1982.

64 Brovkin, V., Ganopolski, A., Archer, D., and Munhoven, G.: Glacial CO<sub>2</sub> cycle as a succession of key physical and  
65 biogeochemical processes, *Clim. Past*, 8, 251-264, <https://doi.org/10.5194/cp-8-251-2012>, 2012.

66 Buchanan, P. J., Matear, R. J., Lenton, A., Phipps, S. J., Chase, Z., and Etheridge, D. M.: The simulated climate of the Last  
67 Glacial Maximum and insights into the global marine carbon cycle, *Clim. Past*, 12, 2271-2295,  
68 <https://doi.org/10.5194/cp-12-2271-2016>, 2016.

69 Bunzel, D., Schmiedl, G., Lindhorst, S., Mackensen, A., Reolid, J., Romahn, S., and Betzler, C.: A multi-proxy analysis of  
70 Late Quaternary ocean and climate variability for the Maldives, Inner Sea, *Clim. Past*, 13, 1791-1813,  
71 <https://doi.org/10.5194/cp-13-1791-2017>, 2017.

72 Burke, A. and Robinson, L. F.: The Southern Ocean's role in carbon exchange during the last deglaciation, *Science*, 335,  
73 557–561, 2012.

74 Chikamoto, M. O., Abe-Ouchi, A., Oka, A., Ohgaito, R., and Timmermann, A.: Quantifying the ocean's role in glacial CO<sub>2</sub>  
75 reductions, *Clim. Past*, 8, 545-563, <https://doi.org/10.5194/cp-8-545-2012>, 2012.

76 Ciais, P., Sabine, C., Bala, G., Bopp, L., Brovkin, V., Canadell, J., Chhabra, A., DeFries, R., Galloway, J., Heimann, M.,  
77 Jones, C., Le Quéré, C., Myneni, R. B., Piao, S., and Thornton, P.: Carbon and Other Biogeochemical Cycles, in:  
78 *Climate Change 2013: The Physical Science Basis. Contribution of Working Group I to the Fifth Assessment Report*  
79 *of the Intergovernmental Panel on Climate Change*, edited by: Stocker, T. F., Qin, D., Plattner, G.-K., Tignor, M.,  
80 Allen, S. K., Boschung, J., Nauels, A., Xia, Y., Bex, V., and Midgley, P. M., Cambridge University Press,  
81 Cambridge, United Kingdom and New York, NY, USA, 465– 570, 2013.

82 Conway, T., Wolff, E., Roethlisberger, R., Mulvaney, R., and Elderfield, H.: Constraints on soluble aerosol iron flux to the  
83 Southern Ocean at the Last Glacial Maximum, *Nature Communications*, 6, 1–9, doi:10.1038/ncomms8850, 2015.

84 Curry, W. B. and Oppo, D. W.: Glacial water mass geometry and the distribution of  $\delta^{13}\text{C}$  of  $\text{CO}_2$  in the western Atlantic  
85 Ocean, *Paleoceanography*, 20, PA1017, doi:10.1029/2004PA001021, 2005.

86 [Deutsch, C., Sigman, D. M., Thunell, R. C., Meckler, A. N., and Haug, G. H.: Isotopic constraints on glacial/interglacial  
87 changes in the oceanic nitrogen budget. \*Global Biogeochem. Cy.\*, 18, GB4012, doi:10.1029/2003GB002189, 2004.](#)

88 Diaz, R. J. and Rosenberg, R.: Spreading dead zones and consequences for marine ecosystems, *Science*, 321, 926–929, 2008.

89 Durand, A., Chase, Z., Noble, T. L., Bostock, H., Jaccard, S. L., Townsend, A. T., Bindoff, N. L., Neil, H., and Jacobsen, G.:  
90 Reduced oxygenation at intermediate depth of the southwest Pacific during the last glacial maximum, *Earth Planet.  
91 Sc. Lett.*, 491, 48–57, 2018.

92 [Duteil, O., Koeve, W., Oeschler, A., Bianchi, D., Galbraith, E., Kriest, I., and Matear, R.: A novel estimate of ocean oxygen  
93 utilisation points to a reduced rate of respiration in the ocean interior. \*Biogeosciences\*, 10\(11\), 7723–7738, doi:  
94 10.5194/bg-10-7723-2013, 2013.](#)

95 Eppley, R. W.: Temperature and phytoplankton growth in the sea, *Fish. B.-NOAA*, 70, 1063–1085, 1972.

96 [Eugster, O., Gruber, N., Deutsch, C., Jaccard, S. L., and Payne, M. R.: The dynamics of the marine nitrogen cycle across the  
97 last deglaciation. \*Paleoceanography\*, 28, 116–129, doi:10.1002/palo.20020, 2013.](#)

98 Fischer, H., Schmitt, J., Luthi, D., Stocker, T. F., Tschumi, T., Parekh, P., Joos, F., Kohler, P., Volker, C., Gersonde, R.,  
99 Barbante, C., Le Floch, M., Raynaud, D., and Wolff, E.: The role of Southern Ocean processes in orbital and  
00 millennial  $\text{CO}_2$  variations – a synthesis, *Quaternary Sci. Rev.*, 29, 193–205, 2010.

01 Galbraith, E. and de Lavergne, C.: Response of a comprehensive climate model to a broad range of external forcings:  
02 relevance for deep ocean ventilation and the development of late Cenozoic ice ages, *Clim. Dynam.*,  
03 <https://doi.org/10.1007/s00382-018-4157-8>, 2018.

04 Galbraith, E. D. and Jaccard, S. L.: Deglacial weakening of the oceanic soft tissue pump: global constraints from  
05 sedimentary nitrogen isotopes and oxygenation proxies, *Quaternary Sci. Rev.*, 109, 38–48,  
06 doi:10.1016/j.quascirev.2014.11.012, 2015.

07 Garcia, H. E., Locarnini, R., Boyer, T., Antonov, J., Baranova, O., Zweng, M., and Johnson, D.: Volume 3: Dissolved  
08 Oxygen, Apparent Oxygen Utilization, and Oxygen Saturation, World Ocean Atlas 2009, S. Levitus, Ed. NOAA  
09 Atlas NESDIS 70, US Government Printing Office, Washington, DC, 344 pp., 2010a.

10 Garcia, H. E., Locarnini, R., Boyer, T., Antonov, J., Zweng, M., Baranova, O., and Johnson, D.: Volume 4: Nutrients  
11 (phosphate, nitrate, silicate), World Ocean Atlas 2009, edited by: Levitus, S., NOAA Atlas NESDIS 71, US  
12 Government Printing Office, Washington, DC, 398 pp., 2010b.

13 Gledhill, M. and Buck, K.: The organic complexation of iron in the marine environment: a review, *Frontiers in*  
14 *Microbiology*, 3, 1–17, doi:10.3389/fmicb.2012.00069, 2012.

15 Gottschalk, J., Skinner, L. C., Lippold, J., Vogel, H., Frank, N., Jaccard, S. L., and Waelbroeck, C.: Biological and physical  
16 controls in the Southern Ocean on past millennial-scale atmospheric CO<sub>2</sub> changes, *Nat. Commun.*, 7, 11539,  
17 doi:10.1038/ncomms11539, 2016.

18 [Heinze, C., Hoogakker, B. A. A., and Winguth, A.: Ocean carbon cycling during the past 130 000 years – a pilot study on](#)  
19 [inverse palaeoclimate record modelling. \*Clim. Past\*, 12, 1949–1978. <https://doi.org/10.5194/cp-12-1949-2016>, 2016.](#)

20 Heuzé, C., Heywood, K. J., Stevens, D. P., and Ridley, J. K.: Southern Ocean bottom water characteristics in CMIP5 models,  
21 *Geophys. Res. Lett.*, 40, 1409–1414, doi:10.1002/grl.50287, 2013.

22 Hoogakker, B. A. A., Elderfield, H., Schmedl, G., McCave, I. N., and Rickaby, R. E. M.: Glacial–interglacial changes in  
23 bottom water oxygen content on the Portuguese margin, *Nat. Geosci.*, 8, 40–43, doi:10.1038/ngeo2317, 2015.

24 Hoogakker, B. A. A., Lu, Z., Umling, N., Jones, L., Zhou, X., Rickaby, R. E. M., Thunell, R., Cartapanis, O., and Galbraith,  
25 E.: Glacial expansion of oxygen-depleted seawater in the eastern tropical Pacific. *Nature*, 562 (7727), 410–413,  
26 doi:10.1038/s41586-018-0589-x, 2018.

27 Ito, A., Myriokefalitakis, S., Kanakidou, M., Mahowald, N. M., Scanza, R. A., Hamilton, D. S., Baker, A. R., Jickells, T.,  
28 Sarin, M., Bikkina, S., Gao, Y., Shelley, R. U., Buck, C. S., Landing, W. M., Bowie, A. R., Perron, M. M. G., Guieu,  
29 C., Meskhidze, N., Johnson, M. S., Feng, Y., Kok, J. F., Nenes, A., and Duce, R. A.: Pyrogenic iron: The missing  
30 link to high iron solubility in aerosols, *Sci. Adv.*, in review, 2019.

31 Ito, T. and Follows, M. J.: Preformed phosphate, soft tissue pump and atmospheric CO<sub>2</sub>, *J. Mar. Res.*, 63, 813–839, 2005.

32 Jaccard, S. L. and Galbraith, E. D.: Large climate-driven changes of oceanic oxygen concentrations during the last  
33 deglaciation, *Nat. Geosci.*, 5, 151–156, doi:10.1038/ngeo1352, 2012.

34 Jaccard, S. L., Hayes, C. T., Hodell, D. A., Anderson, R. F., Sigman, D. M., and Haug, G. H.: Two modes of change in  
35 Southern Ocean productivity over the past million years, *Science*, 339, 1419–1423, 2013.

36 [Jaccard, S. L., Galbraith, E. D., Martínez-García, A., and Anderson, R. F.: Covariation of deep Southern Ocean oxygenation  
37 and atmospheric CO<sub>2</sub> through the last ice age, \*Nature\*, 530, 207–10, doi:10.1038/nature16514, 2016.](#)

38 Key, R. M., Kozyr, A., Sabine, C. L., Lee, K., Wanninkhof, R., Bullister, J. L., Feely, R. A., Millero, F. J., Mordy, C., and  
39 Peng, T.-H.: A global ocean carbon climatology: Results from Global Data Analysis Project (GLODAP), *Global  
40 Biogeochem. Cy.*, 18, GB4031, <https://doi.org/10.1029/2004GB002247>, 2004.

41 Kobayashi, H., Abe-Ouchi, A., and Oka, A.: Role of Southern Ocean stratification in glacial atmospheric CO<sub>2</sub> reduction  
42 evaluated by a three-dimensional ocean general circulation model, *Paleoceanography*, 30, 1202–1216, 2015.

43 Kobayashi, H., and Oka, A.: Response of atmospheric *p*CO<sub>2</sub> to glacial changes in the Southern Ocean amplified by carbonate  
44 compensation. *Paleoceanography* 33, 1206-1229, 2018.

45 Kohfeld, K. E., Le Quéré, C., Harrison, S. P., and Anderson, R. F.: Role of marine biology in glacial-interglacial CO<sub>2</sub>  
46 cycles, *Science*, 308, 74–78, doi:10.1126/science.1105375, 2005.

47 Kohfeld, K. E., Graham, R. M., De Boer, A. M., Sime, L. C., Wolff, E. W., Le Quere, C., and Bopp, L.: Southern  
48 Hemisphere westerly wind changes during the Last Glacial Maximum: paleo-data synthesis, *Quaternary Sci. Rev.*,  
49 68, 76–95, <https://doi.org/10.1016/j.quascirev.2013.01.017>, 2013.

50 Lambert, F., Tagliabue, A., Shaffer, G., Lamy, F., Winckler, G., Farias, L., Gallardo, L., and De Pol-Holz, R.: Dust fluxes  
51 and iron fertilization in Holocene and Last Glacial Maximum climates, *Geophys. Res. Lett.*, 42, 6014–6023,  
52 doi:10.1002/2015gl064250, 2015.

53 Lu, Z., Hoogakker, B. A. A., Hillenbrand, C.-D., Zhou, X., Thomas, E., Gutchess, K. M., Lu, W., Jones, L., and Rickaby, R.  
54 E. M.: Oxygen depletion recorded in upper waters of the glacial Southern Ocean, *Nat. Commun.*, 7, 11146,  
55 <https://doi.org/10.1038/ncomms11146>, 2015.

56 Mahowald, N. M., Muhs, D. R., Levis, S., Rasch, P. J., Yoshioka, M., Zender, C. S., and Luo, C.: Change in atmospheric  
57 mineral aerosols in response to climate: last glacial period, preindustrial, modern, and doubled carbon dioxide  
58 climates, *J. Geophys. Res.*, 111, D10202, doi:10.1029/2005JD006653, 2006.

59 Marinov, I., Gnanadesikan, A., Sarmiento, J. L., Toggweiler, J. R., Follows, M., and Mignone, B. K.: Impact of oceanic  
60 circulation on biological carbon storage in the ocean and atmospheric pCO<sub>2</sub>, *Global Biogeochem. Cy.* 22(3),  
61 GB3007, doi:10.1029/2007GB002958, 2008.

62 Martin, J. H.: Glacial-interglacial CO<sub>2</sub> change: the iron hypothesis, *Paleoceanography*, 5, 1–13, 1990.

63 Matsumoto, K.: Biology-mediated temperature control on atmospheric pCO<sub>2</sub> and ocean biogeochemistry, *Geophys. Res.*  
64 *Lett.*, 34, L20605, <https://doi.org/10.1029/2007GL031301>, 2007.

65 [Menviel, L., Joos, F., and Ritz, S. P.: Simulating atmospheric CO<sub>2</sub>, <sup>13</sup>C and the marine carbon cycle during the Last Glacial-](#)  
66 [Interglacial cycle: possible role for a deepening of the mean remineralization depth and an increase in the oceanic](#)  
67 [nutrient inventory, \*Quat. Sci. Rev.\*, 56, 46-68, 10.1016/j.quascirev.2012.09.012, 2012.](#)

68 Middleton, J. L., Langmuir, C. H., Mukhopadhyay, S., McManus, J. F., and Mitrovica, J. X.: Hydrothermal iron flux  
69 variability following rapid sea level changes, *Geophys. Res. Lett.*, 43, 3848–3856,  
70 <https://doi.org/10.1002/2016GL068408>, 2016.

71 Moore, J. K. and Braucher, O.: Sedimentary and mineral dust sources of dissolved iron to the world ocean, *Biogeosciences*,  
72 5, 631–656, doi:10.5194/bg-5-631-2008, 2008.

73 Moore, C. M., Mills, M. M., Arrigo, K. R., Berman-Frank, I., Bopp, L., Boyd, P. W., Galbraith, E. D., Geider, R. J., Guieu,  
74 C., Jaccard, S. L., Jickells, T. D., La Roche, J., Lenton, T. M., Mahowald, N. M., Marañón, E., Marinov, I., Moore,  
75 J. K., Nakatsuka, T., Oschilles, A., Saito, M. A., Thingstad, T. F., Tsuda, A., and Ulloa, O.: Processes and patterns of  
76 oceanic nutrient limitation, *Nat. Geosci.*, 6, 701–710, <https://doi.org/10.1038/ngeo1765>, 2013.

77 Muglia, J., Somes, C., Nickelsen, L., and Schmittner, A.: Combined effects of atmospheric and seafloor iron fluxes to the  
78 glacial ocean. *Paleoceanography* 32, 1204–1218, 2017.

79 [Muglia, J., Skinner, L. C., and Schmittner A.: Weak overturning circulation and high Southern Ocean nutrient utilization](#)  
80 [maximized glacial ocean carbon, \*Earth Planet Sc Lett.\* 496, 47-56, doi: 10.1016/j.epsl.2018.05.038, 2018.](#)

81 Obase, T., Abe-Ouchi, A., Kushara, K., Hasumi, H., and Ohgaito, R.: Responses of basal melting of Antarctic ice shelves to  
82 the climatic forcing of the Last Glacial Maximum and CO<sub>2</sub> doubling. *J. Climate*, 30, 3473–3497, 2017.

83 Ohgaito, R., Abe-Ouchi, A., O’ishi, R., Takemura, T., Ito, A., Hajima, T., Watanabe, S., and Kawamiya, M.: Effect of high  
84 dust amount on surface temperature during the Last Glacial Maximum: a modelling study using MIROC-ESM,  
85 *Clim. Past*, 14, 1565-1581, <https://doi.org/10.5194/cp-14-1565-2018>, 2018.

86 Oka, A., Abe-Ouchi, A., Chikamoto, M. O., and Ide, T.: Mechanisms controlling export production at the LGM: Effects of  
87 changes in oceanic physical field and atmospheric dust deposition, *Global Biogeochem. Cy.*, 25, GB2009,  
88 doi:10.1029/2009GB003628, 2011.

89 Parekh, P., Follows, M. J., and Boyle, E. A.: Decoupling of iron and phosphate in the global ocean, *Global Biogeochem. Cy.*,  
90 19, GB2020, doi:10.1029/2004GB002280, 2005.

91 Parekh, P., Follows, M. J., Dutkiewicz, S., and Ito, T.: Physical and biological regulation of the soft tissue carbon pump,  
92 *Paleoceanography*, 21, PA3001, doi:10.1029/2005PA001258, 2006.

93 [Parekh, P., Joos, F., and Muller, S. A.: A modeling assessment of the interplay between aeolian iron fluxes and ironbinding  
94 ligands in controlling carbon dioxide fluctuations during Antarctic warm events. \*Paleoceanography\*, 23, Pa4202,  
95 doi:10.1029/2007pa001531, 2008.](#)

96 [Roth, R., Ritz, S. P., and Joos, F.: Burial-nutrient feedbacks amplify the sensitivity of atmospheric carbon dioxide to changes  
97 in organic matter remineralisation. \*Earth Syst. Dynam.\*, 5, 321-343, 10.5194/esd-5-321-2014, 2014.](#)

98 [Russell, J. L., and Dickson, A. G.: Variability in oxygen and nutrients in South Pacific Antarctic Intermediate Water. \*Global  
99 Biogeochem Cy.\* 17, doi:10.1029/2000gb001317, 2003.](#)

00 Sarmiento, J. L., and Gruber, N.: *Ocean Biogeochemical Dynamics*, chap. 8, Carbon cycle, pp.318-358, Princeton Univ.  
01 Press, Princeton, N. J, 2006.

02 Schmiedel, G. and Mackensen, A.: Multispecies stable isotopes of benthic foraminifers reveal past changes of organic matter  
03 decomposition and deepwater oxygenation in the Arabian Sea, *Paleoceanography*, 21, 1–14,  
04 doi:10.1029/2006PA001284, 2006.

05 Schmittner, A. and Somes, C. J.: Complementary constraints from carbon (C-13) and nitrogen (N-15) isotopes on the glacial  
06 ocean's soft-tissue biological pump, *Paleoceanography*, 31, 669–693, 2016.

07 Schroth, A. W., Crusius, J., Sholkovitz, E. R., and Bostick, B. C.: Iron solubility driven by speciation in dust sources to the  
08 ocean, *Nat. Geosci.*, 2, 337–340, 2009.

09 Shoenfelt, E. M., Winckler, G., Lamy, F., Anderson, R. F., and Bostick, B. C.: Highly bioavailable dust-borne iron delivered  
10 to the Southern Ocean during glacial periods. *Proc. Natl. Acad. Sci. USA*, 115, 11180–11185, 2018

11 Sigman, D. M., Hain, M. P., and Haug, G. H.: The polar ocean and glacial cycles in atmospheric CO<sub>2</sub> concentration, *Nature*,  
12 466, 47–55, doi:10.1038/nature09149, 2010.

13 Skinner, L. C., Fallon, S., Waelbroeck, C., Michel, E., and Barker, S.: Ventilation of the deep Southern Ocean and deglacial  
14 CO<sub>2</sub> rise, *Science*, 328, 1147–1151, 2010.

15 [Somes, C. J., Schmittner, A., Muglia, J., and Oschlies A.: A Three-Dimensional Model of the Marine Nitrogen Cycle during  
16 the Last Glacial Maximum Constrained by Sedimentary Isotopes, \*Frontiers in Marine Science\*, 4,  
17 doi:10.3389/fmars.2017.00108, 2017.](#)

18 Tagliabue, A., Bopp, L., Dutay, J. C., Bowie, A. R., Chever, F., Jean-Baptiste, P., Bucciarelli, E., Lannuzel, D., Remenyi, T.,  
19 Sarthou, G., Aumont, O., Gehlen, M., and Jeandel, C.: Hydrothermal contribution to the oceanic dissolved iron  
20 inventory, *Nat. Geosci.*, 3, 252–256, 2010.

21 Tagliabue, A., Bopp, L., Roche, D. M., Bouttes, N., Dutay, J.-C., Alkama, R., Kageyama, M., Michel, E., and Paillard, D.:  
22 Quantifying the roles of ocean circulation and biogeochemistry in governing ocean carbon-13 and atmospheric  
23 carbon dioxide at the last glacial maximum, *Clim. Past*, 5, 695–706, <https://doi.org/10.5194/cp-5-695-2009>, 2009.

24 [Tamburini, F. and Föllmi, K. B.: Phosphorus burial in the ocean over glacial-interglacial time scales, \*Biogeosciences\*, 6,  
25 501–513, doi:10.5194/bg-6-501-2009, 2009.](#)

26 [Tschumi, T., Joos, F., Gehlen, M., and Heinze, C.: Deep ocean ventilation, carbon isotopes, marine sedimentation and the  
27 deglacial CO<sub>2</sub> rise, \*Clim. Past\*, 7, 771–800, 10.5194/cp-7-771-2011, 2011.](#)

28 Umling, N. E., and Thunell, R. C.: Mid-depth respired carbon storage and oxygenation of the eastern equatorial Pacific over  
29 the last 25,000 years. *Quaternary Science Reviews*, 189, 43–56, 2018.

30 Vaquer-Sunyer, R. and Duarte, C. M.: Thresholds of hypoxia for marine biodiversity, *Proc. Natl. Acad. Sci.*, 105, 15452–57,  
31 2008.

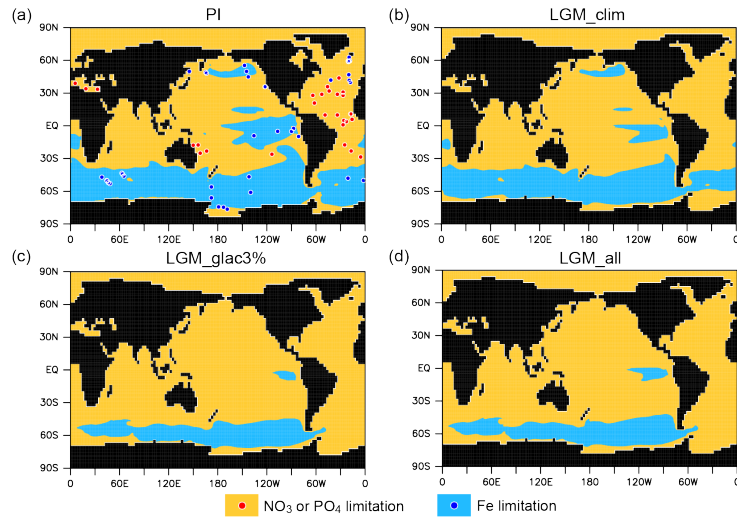
32 Völker, C. and Tagliabue, A.: Modeling organic iron-binding ligands in a three-dimensional biogeochemical ocean model,  
33 *Mar. Chem.*, 173, 67–77, doi:10.1016/j.marchem.2014.11.008, 2015.

34 Wallmann, K., Schneider, B., and Sarnthein, M.: Effects of eustatic sea-level change, ocean dynamics, and nutrient  
35 utilization on atmospheric  $p\text{CO}_2$  and seawater composition over the last 130 000 years: a model study, *Clim. Past*,  
36 12, 339-375, <https://doi.org/10.5194/cp-12-339-2016>, 2016.

37 Yamamoto, A., Abe-Ouchi, A., Shigemitsu, M., Oka, A., Takahashi, K., Ohgaito, R., and Yamanaka, Y.: Global deep ocean  
38 oxygenation by enhanced ventilation in the Southern Ocean under longterm global warming, *Global Biogeochem.*  
39 *Cy.*, 29, 1801–1815, 2015.

40 Yamamoto, A., Abe-Ouchi, A., and Yamanaka, Y.: Long-term response of oceanic carbon uptake to global warming via  
41 physical and biological pumps, *Biogeosciences*, 15, 4163-4180, <https://doi.org/10.5194/bg-15-4163-2018>, 2018.

42  
43  
44

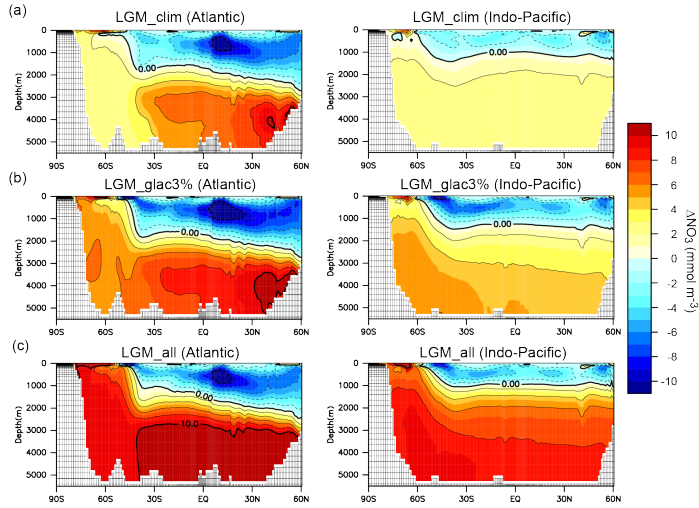


45

46 **Figure 1.** Primary limiting nutrient for phytoplankton for the (a) PI, (b) LGM\_clim, (c) LGM\_glac3%, and (d) LGM\_all.  
 47 Shade indicates NO<sub>3</sub> or PO<sub>4</sub> limitation (orange) and Fe limitation (blue). Circles represent observed limiting nutrients from  
 48 nutrient addition experiments (Moore et al., 2013).

49

削除:

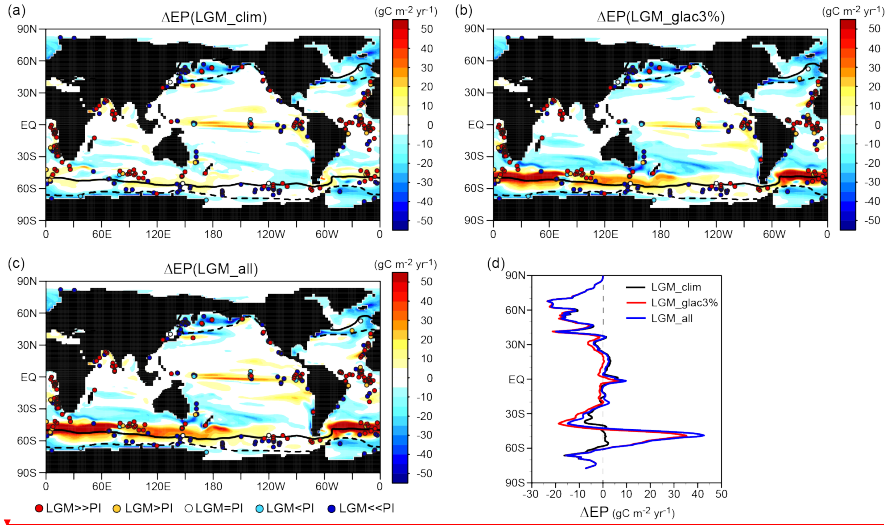


51

52 **Figure 2.**  $\text{NO}_3$  change resulting from changes in the climate and biological pump in LGM simulations. Zonal mean changes  
 53 in  $\text{NO}_3$  from the PI to (a) LGM\_clim, (b) LGM\_glac3%, and (c) LGM\_all. The left and right panels show the Atlantic and  
 54 Indo-Pacific oceans, respectively.

55

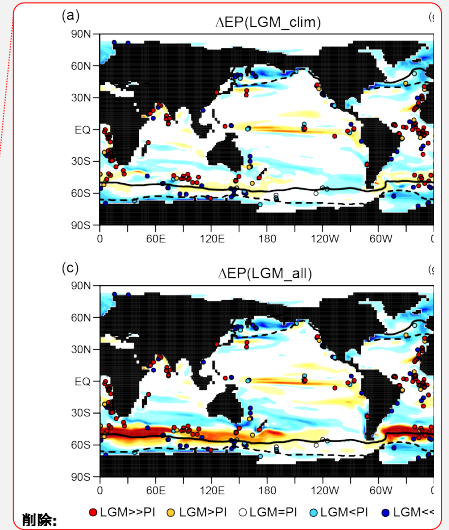
删除: due to



57

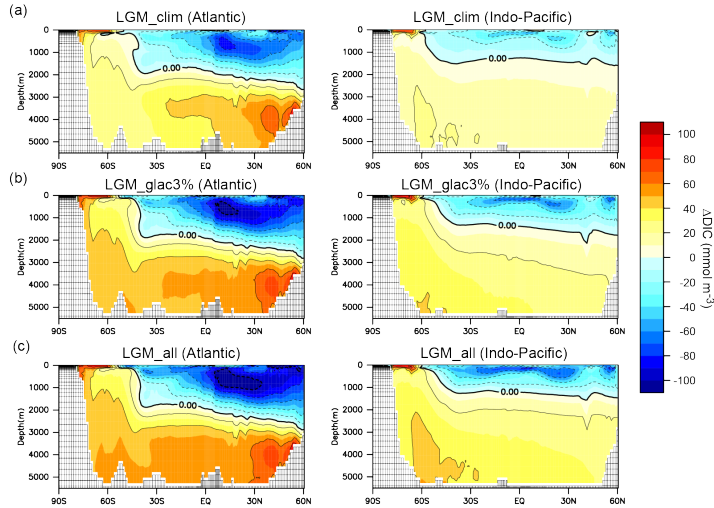
58 **Figure 3.** Model-proxy comparison of EP change from the PI to LGM. **The** EP difference from the PI for (a) LGM\_clim, (b)  
 59 LGM\_glac3%, and (c) LGM\_all. Circles show proxy data (Kohfeld et al., 2013). Solid (dotted) lines refer to the glacial sea  
 60 ice fraction of 0.1 **during** August (February). (d) Zonal mean changes in **the** surface EP from the PI for LGM\_clim (black),  
 61 LGM\_glac3% (red), and LGM\_all (blue).

62



删除: 05

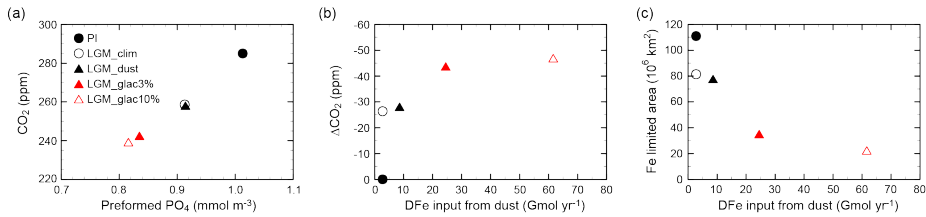
删除: in



66

67 **Figure 4.** DIC change resulting from changes in the climate and biological pump in LGM simulations. Zonal mean changes  
 68 in DIC from PI to (a) LGM\_clim, (b) LGM\_glac3%, and (c) LGM\_all. The left and right panels show the Atlantic and Indo-  
 69 Pacific oceans, respectively.

70



71

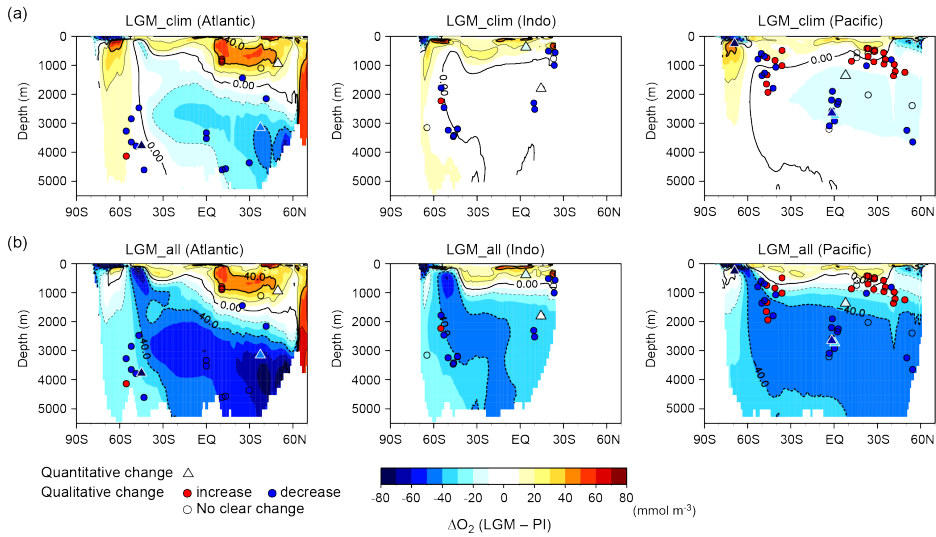
72 **Figure 5.** CO<sub>2</sub> change and its relationship to efficiency of the biological pump and iron cycle. (a) Atmospheric CO<sub>2</sub> as a  
 73 function of globally averaged preformed PO<sub>4</sub>. (b) Changes in CO<sub>2</sub> from the PI as a function of DFe input from dust. (c) Fe-  
 74 limited area as a function of DFe input from dust. Shown are the PI (black filled circle), LGM\_clim (black open circle),  
 75 LGM\_dust (black filled triangle), LGM\_glac3% (red filled triangle), and LGM\_glac10% (red open triangle).

删除: due to

删除:

78

79



80

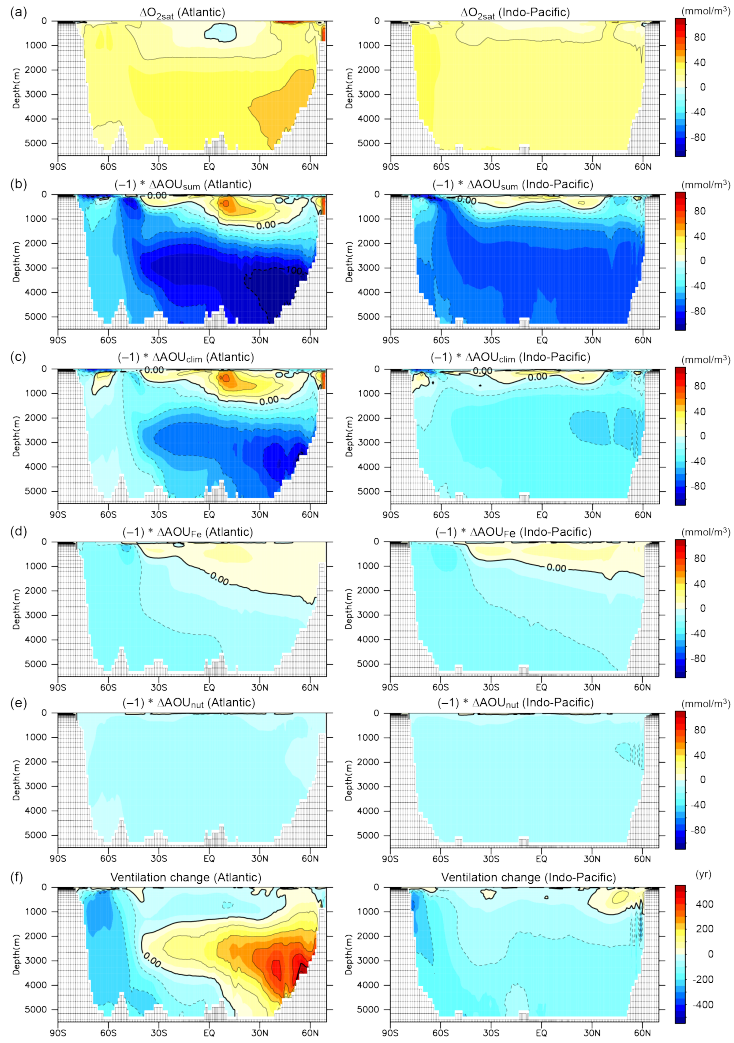
81 **Figure 6.** Model-proxy comparison of changes in dissolved oxygen concentration from the PI to LGM. Zonal mean changes  
 82 in  $O_2$  from the PI to (a) LGM\_clim and (b) LGM\_all for the Atlantic (left), Indian (middle), and Pacific (right) oceans; the  
 83 contour interval is 20 mmol m<sup>-3</sup>. Circles show proxy records of qualitative  $O_2$  change from multi-proxy data compilation from  
 84 Jaccard and Galbraith (2012) (except  $\delta^{15}N$  data), Jaccard et al. (2016), and Durand et al. (2018). Red (blue) circles indicate  $O_2$   
 85 increase (decrease) from the Holocene to LGM. Triangles show proxy records of quantitative  $O_2$  change from (Schmiedl and  
 86 Mackensen, 2006; Hoogakker et al., 2015, 2018; Gottschalk et al., 2016; Lu et al., 2016; Bunzel et al., 2017; Umling and  
 87 Thunell, 2018) (triangles shaded using the same colour scale).

88

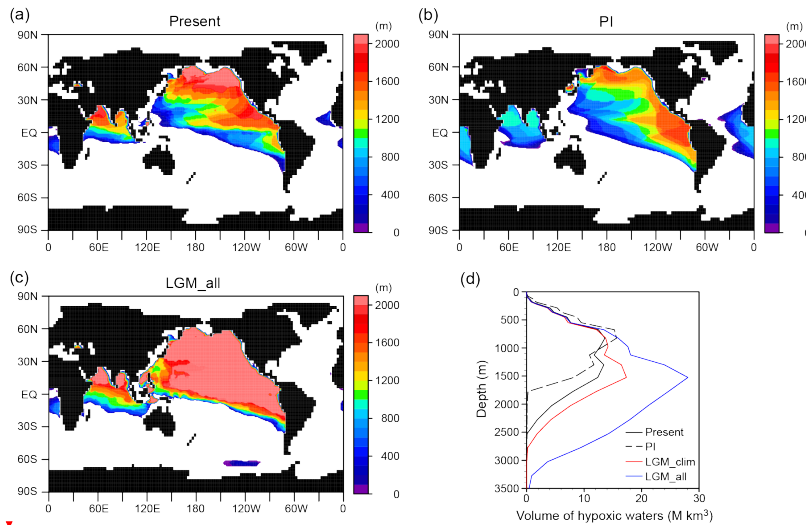
89

删除: O

删除: Schmiedl and Mackensen, 2006



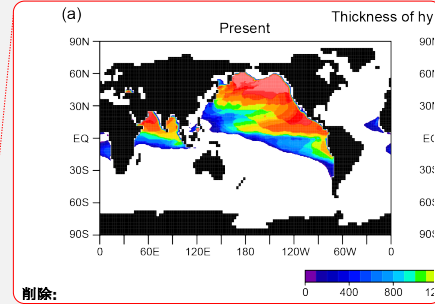
93 **Figure 7.** Contributions of individual mechanisms to oxygen change and ventilation change. Zonal mean changes of (a)  $O_{2sat}$ ,  
 94 (b)  $AOU_{sum}$ , (c)  $AOU_{clim}$ , (d)  $AOU_{Fe}$ , (e)  $AOU_{nut}$ , and (f) ventilation age from the PI to LGM. Left and right panels show the  
 95 Atlantic and Indo-Pacific oceans: the contour intervals are  $20 \text{ mmol m}^{-3}$  for (a)–(e) and 100 years for (f). We decomposed the  
 96 total AOU change ( $\Delta AOU_{sum} = AOU_{(LGM\_all)} - AOU_{(PI)}$ ) into the effects of climate change ( $\Delta AOU_{clim} = AOU_{(LGM\_clim)} -$   
 97  $AOU_{(PI)}$ ), iron fertilization ( $\Delta AOU_{Fe} = AOU_{(LGM\_glac3\%)} - AOU_{(LGM\_clim)}$ ), and nutrient inventory increase ( $\Delta AOU_{nut} =$   
 98  $AOU_{(LGM\_all)} - AOU_{(LGM\_glac3\%)}$ ).



01 **Figure 8.** Hypoxic waters expansion. Horizontal distribution of thickness of the hypoxic waters ( $[O_2] < 80 \text{ mmol m}^{-3}$ ) for the  
 02 (a) present, (b) PI, and (c) LGM all. (d) Vertical distribution of hypoxic waters for the present (black solid), PI (black dashed),  
 03 LGM\_clim (red), and LGM\_all (blue). Because current coarse resolution models have difficulties reproducing low oxygen  
 04 concentration for the present day (Bopp et al., 2013), observed values from WOA2009 (Garcia et al., 2010a) were used for the  
 05 present. For the LGM simulations, we combined the observed values with the modelled changes.

删除: 0

删除: increase in



删除:

删除: Expansion of h

删除: b

删除: c

删除: present

删除: in

删除: a

| Experiments | Climate | Dust deposition | Fe solubility in glaciogenic dust | Dust DFe (Gmol yr <sup>-1</sup> ) | Global PO <sub>4</sub> (mmol m <sup>-3</sup> ) |
|-------------|---------|-----------------|-----------------------------------|-----------------------------------|--|
| PI          | PI      | PI              | -                                 | 2.7                               | 2.13   |
| LGM_clim    | LGM     | PI              | -                                 | 2.7                               | 2.2 (+3%)                                      |
| LGM_dust    | LGM     | LGMctl          | -                                 | 8.6                               | 2.2 (+3%)                                      |
| LGM_glac3%  | LGM     | LGMglac         | 3%                                | 24.5                              | 2.2 (+3%)                                      |
| LGM_glac10% | LGM     | LGMglac         | 10%                               | 61.6                              | 2.2 (+3%)                                      |
| LGM_all     | LGM     | LGMglac         | 3%                                | 24.5                              | 2.45 (+15%)                                    |

| Experiments | Climate | Dust deposition | Fe sol |
|-------------|---------|-----------------|--------|
| PI          | PI      | PI              |        |
| LGM_clim    | LGM     | PI              |        |
| LGM_dust    | LGM     | LGMctl          |        |
| LGM_glac3%  | LGM     | LGMglac         |        |
| LGM_glac10% | LGM     | LGMglac         |        |
| LGM_all     | LGM     | LGMglac         |        |

削除:

Table 1. Description of the model experiments.

| Experiments | Surface NO <sub>3</sub> (mmol m <sup>-3</sup> ) | Surface DFe (μmol m <sup>-3</sup> ) | Fe limited area (10 <sup>6</sup> km <sup>2</sup> ) | Global ΔEP (Pg C yr <sup>-1</sup> ) | ΔEP (>45°S) (Pg C yr <sup>-1</sup> ) | ΔEP (<45°S) (Pg C yr <sup>-1</sup> ) | Preformed PO <sub>4</sub> (mmol m <sup>-3</sup> ) | ΔCO <sub>2</sub> (ppm) | ΔO <sub>2,dep</sub> (mmo m <sup>-3</sup> ) | ΔAOU <sub>dep</sub> (mmol m <sup>-3</sup> ) |
|-------------|---|-------------------------------------|--|-------------------------------------|--------------------------------------|--------------------------------------|---|------------------------|--|---|
| PI          | 7.7   | 0.38                                | 111  | (8.54)                              | (6.19)                               | (2.35)                               | 1.013   | (285)                  | (156)                                      | (182.5)                                     |
| LGM_clim    | 6.8   | 0.39                                | 81   | -0.54                               | -0.45                                | -0.09                                | 0.913   | -26.4                  | -7   | 37.3  |
| LGM_dust    | 6.9   | 0.42                                | 80   | -0.54                               | -0.49                                | -0.05                                | 0.914   | -27.6                  | -8   | 38.9  |
| LGM_glac3%  | 5.8   | 0.5                                 | 35   | -0.54                               | -1.31                                | +0.77                                | 0.835   | -43.2                  | -28  | 58.7  |
| LGM_glac10% | 5.5   | 0.54                                | 23   | -0.54                               | -1.46                                | +0.92                                | 0.816   | -46.4                  | -33  | 63.6  |
| LGM_all     | 6.5   | 0.48                                | 39   | +0.32                               | -0.63                                | +0.95                                | 1.002   | -59.2                  | -42  | 72.8  |

| Experiments | Surface NO <sub>3</sub> (mmol/m <sup>3</sup> ) | Surface DFe (μmol/m <sup>3</sup> ) | Fe limited area (10 <sup>6</sup> km <sup>2</sup> ) |
|-------------|--|------------------------------------|--|
| PI          | 7.7  | 0.38                               | 111  |
| LGM_clim    | 6.8  | 0.39                               | 81   |
| LGM_dust    | 6.9  | 0.42                               | 80   |
| LGM_glac3%  | 5.8  | 0.5                                | 35   |
| LGM_glac10% | 5.5  | 0.54                               | 23   |
| LGM_all     | 6.5  | 0.48                               | 39   |

削除:

Table 2. Results of the model experiments. Simulated global average of surface NO<sub>3</sub>, DFe, and Fe<sub>2</sub> limited area and changes in

EP at 100 m, atmospheric CO<sub>2</sub>, and globally averaged preformed PO<sub>4</sub>, O<sub>2</sub> and AOU below 2000 m depth from the PI. Values in brackets are the PI results.

削除:

削除: export production

書式変更: 下付き

削除: results of